

การเตรียมชั้นกั้นการแพร่โครเมียมออกไซด์และโครเมียมไนไตรด์สำหรับแพลตฟอร์มเมมเบรนบน
ตัวรองรับเหล็กกล้าไร้สนิม

นางสาว สรัญญา พลอยประดับ

วิทยานิพนธ์นี้เป็นส่วนหนึ่งของการศึกษาตามหลักสูตรปริญญาวิทยาศาสตรมหาบัณฑิต
สาขาวิชาปิโตรเคมีและวิทยาศาสตร์พอลิเมอร์
คณะวิทยาศาสตร์ จุฬาลงกรณ์มหาวิทยาลัย
ปีการศึกษา 2552
ลิขสิทธิ์ของจุฬาลงกรณ์มหาวิทยาลัย

PREPARATION OF Cr₂O₃ AND CrN DIFFUSION BARRIERS FOR STAINLESS
STEEL SUPPORTED PALLADIUM MEMBRANE

Miss Saranya Ploypardup

A Thesis Submitted in Partial Fulfillment of the Requirements
for the Degree of Master of Science Program in Petrochemistry and Polymer Science
Faculty of Science
Chulalongkorn University
Academic year 2009
Copyright of Chulalongkorn University

Thesis Title PREPARATION OF Cr₂O₃ AND CrN DIFFUSION
BARRIERS FOR STAINLESS STEEL SUPPORTED
PALLADIUM MEMBRANE

By Miss. Saranya Ploypardup

Field of Study Petrochemistry and Polymer Science

Thesis Advisor Associate Professor Supawan Tantayanon, Ph.D.

Thesis Co-Adviser Assistant Professor Sukkaneste Tungasmita, Ph.D.

Accepted by the Faculty of Science, Chulalongkorn University in Partial
Fulfillment of the Requirements for the Master's Degree

..... Dean of the Faculty of Science
(Professor Supot Hannongboa, Dr.rer.nat.)

THESIS COMMITTEE

..... Chairman
(Professor Pattarapan Prasassarakich, Ph.D.)

..... Thesis Advisor
(Associate Professor Supawan Tantayanon, Ph.D.)

..... Thesis Co-Adviser
(Assistant Professor Sukkaneste Tungasmita, Ph.D.)

..... Examiner
(Assistant Professor Warinthron Chavasiri, Ph.D.)

..... External Examiner
(Ratchatee Techapiesancharoenkij, Ph.D.)

สรุปัญญา พลอยประดับ: การเตรียมชั้นกั้นการแพร่โครเมียมออกไซด์และโครเมียมไนไตรด์ สำหรับแพลเลเดียมเมมเบรนบนตัวรองรับเหล็กกล้าไร้สนิม (PREPARATION OF Cr_2O_3 AND CrN DIFFUSION BARRIERS FOR STAINLESS STEEL SUPPORTED PALLADIUM MEMBRANE) อ.ที่ปรึกษาวิทยานิพนธ์หลัก: รศ.ดร. ศุภวรรณ ตันตยานนท์, อ.ที่ปรึกษาวิทยานิพนธ์ร่วม: ผศ.ดร.สุคนธ์เดช ตุงคสมิต, 73 หน้า

ในงานวิจัยนี้ได้ศึกษาการนำฟิล์มบางโครเมียมออกไซด์และโครเมียมไนไตรด์มาเป็นชั้นกั้นการแพร่โลหะระหว่างแพลเลเดียมเมมเบรนและตัวรองรับเหล็กกล้าไร้สนิม โดยเตรียมชั้นโครเมียมออกไซด์หลายรูปแบบ เช่น การออกซิไดซ์ด้วยความร้อนโดยตรง, การออกซิไดซ์ชั้นโครเมียมที่สร้างจากกระบวนการอิเล็กโทรเพลทติง, การออกซิไดซ์ชั้นโครเมียมที่สร้างจากกระบวนการสปัตเตอริงโลหะโครเมียม ซึ่งความหนาของชั้นโครเมียมขึ้นอยู่กับเวลาที่ใช้ในการเตรียมฟิล์มบาง และสามารถตรวจวัดได้จากเทคนิคการชั่งน้ำหนักและกล้องจุลทรรศน์อิเล็กตรอนแบบส่องกราด พบว่าความหนาของชั้นโครเมียมที่ตรวจวัดด้วยกล้องจุลทรรศน์อิเล็กตรอนแบบส่องกราดมีความหนาระหว่าง 1-6 ไมโครเมตร และภาวะที่เหมาะสมในการออกซิไดซ์ชั้นโครเมียมให้กลายเป็นโครเมียมออกไซด์ คือที่อุณหภูมิ 600 องศาเซลเซียสเป็นเวลา 6 ชั่วโมง และเตรียมชั้นฟิล์มบางโครเมียมไนไตรด์โดยการสปัตเตอริงโลหะโครเมียมในบรรยากาศไนโตรเจน สามารถตรวจสอบหาค่าประกอบและลักษณะโครงสร้างของชั้นกั้นการแพร่ที่เตรียมโดยเทคนิควิเคราะห์ธาตุเชิงพลังงานและการเลี้ยวเบนรังสีเอกซ์ จากนั้นเตรียมแพลเลเดียมเมมเบรนบนชั้นกั้นที่เตรียมได้ด้วยเทคนิคอิเล็กโทรเพลทติง ทดสอบประสิทธิภาพการป้องกันการแพร่โดยวิเคราะห์ธาตุองค์ประกอบที่พบในชั้นแพลเลเดียมหลังจากที่ให้ความร้อนในบรรยากาศไฮโดรเจนที่อุณหภูมิ 400, 500 และ 600 องศาเซลเซียสเป็นเวลา 24 ชั่วโมง ด้วยกล้องจุลทรรศน์อิเล็กตรอนแบบส่องกราดที่เชื่อมต่อกับเทคนิควิเคราะห์ธาตุเชิงพลังงาน พบว่าหลังจากให้ความร้อนชั้นกั้นการแพร่ทั้งหมดที่เตรียมได้สามารถป้องกันการแพร่ของโลหะในเหล็กกล้าไร้สนิมเข้าสู่ชั้นแพลเลเดียมได้ และโครเมียมออกไซด์ที่เตรียมได้จากเทคนิคสปัตเตอริงให้อัตราการไหลของแก๊สไฮโดรเจนมากที่สุดเมื่อนำมาทดสอบประสิทธิภาพการแพร่ผ่านของแก๊สไฮโดรเจนที่อุณหภูมิ 350-500 องศาเซลเซียสที่ความดัน 1-3 บรรยากาศ

สาขาวิชา...ปิโตรเคมีและวิทยาศาสตร์พอลิเมอร์.....ลายมือ initials.....

ปีการศึกษา.....2552.....ลายมือชื่ออาจารย์ที่ปรึกษา.....

ลายมือชื่ออาจารย์ที่ปรึกษาร่วม.....

5072631223: MAJOR PETROCHEMISTRY AND POLYMER SCIENCE

KEYWORD: INTERMETALLIC DIFFUSION / CHROMIUM OXIDE / ELECTROLESS
PLATING / CHROMIUM SPUTERRING

SARANYA PLOYPARDUP: PREPARATION OF Cr_2O_3 AND CrN DIFFUSION
BARRIERS FOR STAINLESS STEEL SUPPORTED PALLADIUM MEMBRANE
THESIS ADVISER: ASSOC. PROF. SUPAWAN TANTAYANON, Ph.D., THESIS
CO-ADVISER: ASST. PROF. SUKKANESTE TUNGASMITA, Ph.D., 73 pp.

In this research, chromium oxide (Cr_2O_3) and chromium nitride (CrN) thin films were fabricated as the intermetallic diffusion barriers between the palladium (Pd) membrane and stainless steel (SS) support. Three different methods for preparation of Cr_2O_3 were investigated, i.e., thermal oxidation, oxidized Cr-electroplating, and oxidized Cr-sputtering. The thickness of chromium thin films was controlled by chromium deposition time and measured by gravimetric method and SEM. They were found to be 2 to 6 μm as determined by SEM. The optimum condition for the oxidation of chromium to Cr_2O_3 was at 600°C for 6 hours. The CrN thin film was formed by Cr-sputtering in nitrogen atmosphere. The composition and phase structures of Cr-based thin films were studied by EDS and XRD. The Pd membranes were then developed on top of Cr-based thin films by electroless plating. The efficacies in preventing intermetallic diffusion were assessed employing SEM-EDS to analyze the elemental content of the palladium layer after hydrogen exposure for 24 hours at 400, 500 or 600°C . After the hydrogen exposure, all Cr-based thin films acted as the good intermetallic diffusion barriers, with no detectable presence of elementals from the SS disk on Pd layer. Among the four types of thin films, Cr_2O_3 created by sputtering and oxidation showed the highest permeation flux which was measured at $350\text{-}500^\circ\text{C}$ in pressure differences of 1-3 atm.

Department: Student's Signature

Field of Study: Petrochemistry and Polymer Science Advisor's Signature

Academic Year: 2009 Co-Advisor's Signature

ACKNOWLEDGEMENTS

First of all I would like to express my sincere gratitude and appreciation to my adviser, Associate Professor Supawan Tantayanon, for her support, guidance, and encouragement throughout my education at Chulalongkorn University. She has given me the great opportunity for everything. I also would like to thank my co-adviser, Assistant Professor Sukkaneste Tungasmita, who helped and gave the thin film sputter knowledge. His wealth of information and input has been proved invaluable to this project. Moreover, I would like to thank my committee members, Professor Pattarapan Prasassarakich, Assistant Professor Warinthron Chavasiri, and Dr. Ratchatee Techapiesanchaenokij. I would like to thank National Center of Excellence for Petroleum, Petrochemicals, and Advance Materials (NCE-PPAM), TRF Master Research Grants (TRF-MAG), Photonic Technology Laboratory of National Metal and National Electronics and Computer Technology Center (NECTEC), and Bangkok Industrial Gas Co., Ltd. for the support.

Next, I would like to thank to Mrs. Thitinat Sukonket and Mr. Sutheerawat Samingprai for teaching and give me good suggestion. Let me also thanks to all my friends at greenchemistry laboratory especially, Miss Wanrudee Temnil, Miss Chantimas Tochai, Miss Maslin Chotirat and Miss Thanyaporn Rumpuey. Without their encouragement I could not have finished this dissertation.

Last but not the least; I would like to thank my parents and my family for all the love, trust, support, worries and encouragement. Their great influence made me who I am today.

CONTENTS

	Page
ABSTRACT IN THAI	iv
ABSTRACT IN ENGLISH.....	v
ACKNOWLEDGEMENTS.	vi
CONTENTS.....	vii
LIST OF TABLES.....	x
LIST OF FIGURES.....	xi
LIST OF ABBREVIATIONS.....	xvi
CHAPTER I: INTRODUCTION.....	1
1.1 Introduction.....	1
1.2 Objective	2
CHAPTER II: THEORETICAL STUDIES AND LITERATURE	
REVIEW.....	3
2.1 Hydrogen permeable Membrane	3
2.2 Intermetallic diffusion barrier	4
2.2.1 Electroplating	4
2.2.2 Electroless plating.....	6
2.2.3 Sputtering.....	7
2.3 Literature Reviews	8
CHAPTER III: EXPERIMENTAL.....	15
3.1 Materials, Equipments and Instruments.....	15

	Page
3.1.1 Materials.....	15
3.1.2 Equipments	16
3.1.3 Instruments	16
3.2 Experimental Procedures	16
3.2.1 Preparation of intermetallic diffusion barrier and palladium membrane.....	16
3.2.1.1 Preparation of supports	16
3.2.1.1.1 Surface cleaning with alkaline solution	17
3.2.1.1.2 Surface cleaning with commercial solvent	17
3.2.1.2 Preparations of Cr-based intermetallic diffusion barriers	17
3.2.1.2.1 Thermal oxidation (TO).....	18
3.2.1.2.2 Electroplating (EP)	18
3.2.1.2.3 Magnetron Sputtering (MS).....	18
3.2.1.3 Electroless plating of palladium membranes	19
3.2.1.3.1 Surface activation	20
3.2.1.3.2 Palladium electroless plating	21
3.2.2 Intermetallic diffusion tests.....	21
3.2.3 Hydrogen permeation flux testing.....	22
CHAPTER IV: RESULTS AND DISCUSSION.....	23
4.1 Preparation of intermetallic diffusion barrier and palladium membran.....	23

	Page
4.1.1 Characterization of support	23
4.1.2 Preparation of Cr-based intermetallic diffusion barrier	24
4.1.2.1 Chromium oxide by thermal oxidatio.....	24
4.1.2.2 Chromium oxide electroplating.....	29
4.1.2.3 Chromium oxide by magnetron sputtering.....	33
4.1.2.4 Chromium nitride by magnetron sputtering	35
4.1.3 Electroless plating of palladium membrane	37
4.2 Intermetallic diffusion tests	38
4.3 Hydrogen permeation flux testing.....	46
CHAPTER V: CONCLUSIONS AND SUGGESTIONS.....	54
5.1 Further works.....	55
REFERENCES.....	56
APPENDICES.....	60
VITAE.....	73

LIST OF TABLES

	Page
Table 3.1 Composition of the alkaline solution.....	17
Table 3.2 Chemical composition of activation bath	21
Table 3.3 The composition of electroless palladium plating solution	21
Table 4.1 Elemental compositions of SS and PSS supports.....	23
Table 4.2 Deposition rate of Cr-electro plating	30
Table 4.3 Experimental condition for deposition of Cr coating	33
Table 4.4 Experimental condition for deposition of CrN coating	35
Table 4.5 The preparation conditions of the intermetallic diffusion barriers.....	39
Table 4.6 The preparation conditions of the intermetallic diffusion barriers	46

LIST OF FIGURES

		Page
Figure 2.1	Principle of hydrogen separation through metal membrane	3
Figure 2.2	Schematic of chromium electroplating	5
Figure 2.3	Shows a schematic of a basic DC sputtering system.....	8
Figure 3.1	The chromium electroplating device.....	18
Figure 3.2	Schematic of a basic DC sputtering deposition system.....	19
Figure 3.3	Schematic of genral procedure for palladium plating.....	20
Figure 3.4	Scheme the procedure for surface activation step.....	20
Figure 3.5	Schematic of the permeator cell.....	22
Figure 4.1	The SEM micrograph of stainless steel (SS) support (a), and (b) of porous stainless steel (PSS) support.....	24
Figure 4.2	SEM micrographs of the surface of SS disks before (a) and after oxidation in air at 500°C (b, c), 600°C (d, e), 700°C (f, g) for 6 hrs.....	25
Figure 4.3	The X-ray diffraction patterns of the SS support and TO- Cr ₂ O ₃ /SS after oxidized in 6 hours (a) and 8 hours (b).....	27
Figure 4.4	EDS spectra of SS disks after oxidized at 600 (a) and 700°C (b) for 6 hours.....	28
Figure 4.5	Ratio of Fe/Cr obtained from EDS spot scan analysis of the surface of the oxidized SS disks.....	29

	Page
Figure 4.6 The X-ray diffraction patterns of the Cr thin film on SS support after oxidized in 6 hours (a) and 8 hours (b).....	31
Figure 4.7 SEM micrograph surfaces of Cr-thin film by EP method (EP-Cr/SS) after oxidation 500°C (a, b, c), 600°C (d, e, f), 700°C (g, h, i) for 6 hours.....	32
Figure 4.8 SEM micrograph surfaces of Cr-thin film by MS method after oxidation 600°C (a), 700°C (b) for 6 hours.....	34
Figure 4.9 The X-ray diffraction patterns of the Cr thin film on SS disks after oxidized in 6 hours.....	34
Figure 4.10 X-ray diffraction patterns of the CrN thin film.....	36
Figure 4.11 SEM micrograph surfaces of CrN thin film by reactive magnetron sputtering method	36
Figure 4.12 SEM micrographs of SS disk (a) and palladium layer on SS disk (b).....	37
Figure 4.13 SEM micrograph (a) and EDS line scans (b) of Pd membrane in fresh state.....	38
Figure 4.14 SEM micrograph (a) and EDS line scans (b) of Pd/PSS non barrier (disk #03) after hydrogen exposure at 600°C for 24 hours.....	40
Figure 4.15 SEM micrograph (a) and EDS line scans (b) of Pd/TO-Cr ₂ O ₃ /SS (disk #06) after hydrogen exposure at 600°C for 24 hours.....	41

	Page
Figure 4.16 SEM micrograph (a) and EDS line scans (b) of Pd/EP - Cr ₂ O ₃ /SS (disk #12) after hydrogen exposure at 600°C for 24 hours.....	42
Figure 4.17 SEM micrograph (a) and EDS line scans (b) of Pd/MS-Cr ₂ O ₃ /SS (disk #15) after hydrogen exposure at 600°C for 24 hours.....	43
Figure 4.18 SEM micrograph (a) and EDS line scans (b) of Pd/MS-Cr ₂ O ₃ /SS (disk #18) after hydrogen exposure at 600°C for 24 hours.....	44
Figure 4.19 SEM micrograph (a) and EDS line scans (b) of Pd/MS-CrN/SS (disk #24) after hydrogen exposure at 600°C for 24 hours.....	45
Figure 4.20 SEM micrograph of surface in the Pd/PSS non barrier (a, b) and Pd/TO-Cr ₂ O ₃ /PSS (c, d).....	47
Figure 4.21 SEM micrograph of the Pd/TO-Cr ₂ O ₃ /PSS (a, b), Pd/EP-Cr ₂ O ₃ /PSS (c, d), and Pd/MS-Cr ₂ O ₃ /PSS (e, f).....	48
Figure 4.22 Permeation measurements at different temperature for Pd/PSS (a), Pd/TO-Cr ₂ O ₃ /PSS (b), Pd/EP-Cr ₂ O ₃ /PSS (c), Pd/MS-Cr ₂ O ₃ /PSS (d), and Pd/MS-Cr ₂ O ₃ /PSS (e).....	50
Figure 4.23 Permeation measurements to the of the hydrogen pressures for Pd/PSS (a), Pd/TO-Cr ₂ O ₃ /PSS (b), Pd/EP-Cr ₂ O ₃ /PSS (c), Pd/MS-Cr ₂ O ₃ /PSS (d), and Pd/MS-Cr ₂ O ₃ /PSS (e).....	51

	Page	
Figure 4.24	The linear relationship between the hydrogen pressure difference and the flux (a) and the hydrogen flux of the square root of the hydrogen pressure (b) for disk all samples.....	53
Figure A1	The EDS spectrum for EP-Cr ₂ O ₃ -500°C/SS (a), EP-Cr ₂ O ₃ -600°C/SS (b) and EP-Cr ₂ O ₃ -700°C/SS (c).....	61
Figure A2	The EDS line scans of Pd membrane samples in fresh state (a) and after treatment at 400° (b), 500° (c), and 600°C (d) after 24 hours.....	62-63
Figure A3	The EDS line scans of Pd/EP-Cr ₂ O ₃ -1.0 min-600°C/SS membrane samples after 24 h hydrogen exposure at 400° (a), 500° (b), and 600°C (c).....	64
Figure A4	The EDS line scans of Pd/EP-Cr ₂ O ₃ -0.5 min-600°C/SS membrane samples after 24 h hydrogen exposure at 400° (a), 500° (b), and 600°C (c).....	65
Figure A5	The EDS line scans of Pd/MS-Cr ₂ O ₃ -45 min-600°C/SS membrane samples after 24 h hydrogen exposure at 400° (a), 500° (b), and 600°C (c).....	66
Figure A6	The EDS line scans of Pd/MS-Cr ₂ O ₃ -15 min-600°C/SS membrane samples after 24 h hydrogen exposure at 400° (a), 500° (b), and 600°C (c).....	67
Figure A7	The EDS line scans of Pd/MS-CrN-60 min/SS membrane samples after 24 h hydrogen exposure at 400° (a), 500° (b), and 600°C (c).....	68

	Page
Figure A8 The EDS line scans of Pd/MS-CrN-30 min/SS membrane samples after 24 h hydrogen exposure at 400° (a), 500° (b), and 600°C (c).....	69
Figure A9 The linear relationship between the hydrogen pressure difference and the flux (a) and the hydrogen flux of the square root of the hydrogen pressure (b) for disk #25.....	70
Figure A10 The linear relationship between the hydrogen pressure difference and the flux (a) and the hydrogen flux of the square root of the hydrogen pressure (b) for disk #26.....	70
Figure A11 The linear relationship between the hydrogen pressure difference and the flux (a) and the hydrogen flux of the square root of the hydrogen pressure (b) for disk #27.....	71
Figure A12 The linear relationship between the hydrogen pressure difference and the flux (a) and the hydrogen flux of the square root of the hydrogen pressure (b) for disk #28.....	71
Figure A13 The linear relationship between the hydrogen pressure difference and the flux (a) and the hydrogen flux of the square root of the hydrogen pressure (b) for disk #29.....	72

LIST OF ABBREVIATION

XRD	X-ray diffraction
SEM	Scanning electron microscope
EDS	Energy Dispersive Spectrometer
°C	Degree Celsius
g	gram
eV	Electron volt
mL	Milliliter

CHAPTER I

INTRODUCTION

1.1 Introduction

Hydrogen has become one of the key energy resources of the future and the increasing demand in various chemical and petrochemical industries. There are several ways to produce hydrogen from the reaction of dehydrogenations, the water gas shift, steam reforming and aromatization. They are increasingly used in membrane reactors for reaction where in situ removal of the produced hydrogen from the reaction atmosphere eliminates the equilibrium constraint. Dense palladium received special attention because of their high hydrogen permeability, infinite hydrogen selectivity, and chemical compatibility with many hydrocarbon-containing gas streams [1-2]. Palladium membranes reactors consisting of a thin Pd film supported on a porous substrate (such as vycor glass, ceramic, stainless steel, quartz, etc. [3-8]) is a good alternative that provides both mechanical strength and a thin separation layer for a high hydrogen flux and reduced Pd cost. The most Pd membranes supported on stainless steel because their various advantages such as: good mechanical strength, less fragile and resistant to cracking [9-11]. Although it has been shown that palladium membranes can also be plated directly on porous stainless steel support, this is problematic because intermetallic diffusion of stainless steel elements (mostly Fe, Cr, and Ni) into Pd layer can cause degradation of hydrogen permeability and, finally, membrane failure.

Intermetallic diffusion can be mitigated by forming or depositing an oxide or a high melting point metal layer on the support. Several studies have demonstrated of intermetallic diffusion barrier for Pd membrane. Intermetallic diffusion barriers can be formed by oxidation in air [12], deposition of ceramic layer (ZrO_2 , YSZ, and TiO_2) [13], deposition Pd-Ag composite layer by bi-metal multi-layer (BMML) [14].

1.2Objective

The main objective of the present work is to study the structure resulted from deposited Cr-based thin film on stainless steel and to investigate their effectiveness as an intermetallic diffusion barrier. In orders to prevent intermetallic diffusion, different approaches Cr₂O₃ thin films creating as an intermetallic diffusion barrier by thermal oxidation (TO), electroplating (EP), magnetron sputtering (MS) and CrN thin film by reactive magnetron sputtering on stainless steel support.

CHAPTER II

THEORETICAL AND LITERATURE REVIEW

2.1 Hydrogen permeable Membranes

Gas separation at high temperature is very attractive since many petrochemical processes could be enhanced by gas separation with membrane at operating condition. Metal membrane made of palladium can be used to sieve hydrogen from mixed gas. The hydrogen permeation through a palladium (Pd) membrane is a 5 steps, adsorption of hydrogen molecules on the membrane surface, dissociation into atomic hydrogen on the membrane surface, diffusion of atomic hydrogen through the membrane layer, recombining of H₂ atoms back into H₂ molecules at the permeate side, and desorption of hydrogen molecules from surface of the membrane. Figure 2.1 shows the multi step hydrogen permeation process.

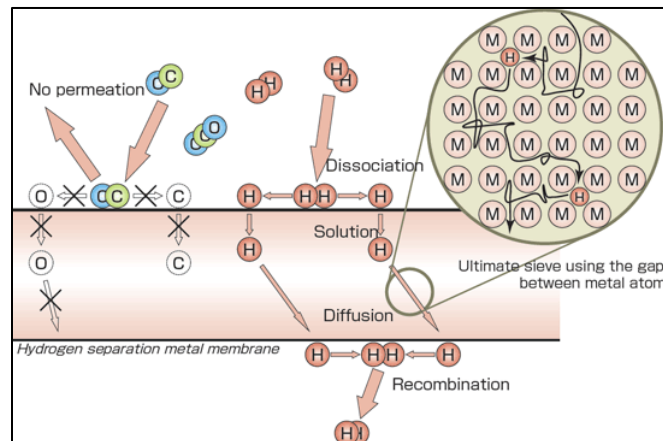


Figure 2.1 Principle of hydrogen separation through metal membrane

The hydrogen permeation is inversely proportional to the film thickness. On the other hand, thinner films have low mechanical strength and low selectivity at higher temperature. Pd membranes consisting of a thin film supported on a porous substrate is an alternative that provides both the mechanical strength and thin

separation layer. Vycor glass, ceramics, porous stainless steel, quartz and other metals in porous form are some alternatives for substrates.

The support is required to have good mechanical and thermal stabilities and also to be produced easily and economically. Porous stainless steel might be a good choice due to its similar thermal expansion coefficient to the Pd films, ease of fabrication and processing, corrosion resistance to crack, and low cost.

However, atomic interdiffusion of metals between the Pd film and the substrate materials occurring at high temperature can deteriorate the performance of the Pd membrane.

2.2 Intermetallic diffusion barrier

Intermetallic diffusion is the migration of the elements in the support into the Pd layer, thereby affecting the H₂ permeance of the membrane. Intermetallic diffusion can be mitigated by forming or depositing an oxide or a high melting point metal layer on the support.

Plating describes surface-covering where a metal is deposited on a conductive surface. Plating is used to decorate objects, for corrosion inhibition, to improve solder ability, to harden, to improve wear ability, to reduce friction, to improve paint adhesion, to alter conductivity, for radiation shielding, and for other purposes. There are several plating methods, and many variations.

2.2.1 Electroplating

In electroplating, an ionic metal is supplied with electrons to form a non-ionic coating on a substrate. A common system involves a chemical solution with the ionic form of the metal, an anode (positively charged) which may consist of the metal being plated (a soluble anode) or an insoluble anode (usually carbon, platinum, titanium, lead, or steel), and finally, a cathode (negatively charged) where electrons are supplied to produce a film of non-ionic metal. The film is affected by several parameters, such as current density, temperature of the electrolyte, migration and

diffusion velocity of ions, specific weight of ions, geometric form of cathode and the both composition.

Chrome plating is a finishing treatment utilizing the electrolytic deposition of chromium. The most common form of chrome plating is the thin, decorative *bright chrome*, which is typically a 10 μm layer over an underlying nickel plate. When plating on iron or steel, an underlying plating of copper allows the nickel to adhere. The pores (tiny holes) in the nickel and chromium layers also promote corrosion resistance. Bright chrome imparts a mirror-like finish to items such as metal furniture frames and automotive trim. Thicker deposits, up to 1000 μm , are called *hard chrome* and are used in industrial equipment to reduce friction and wear.

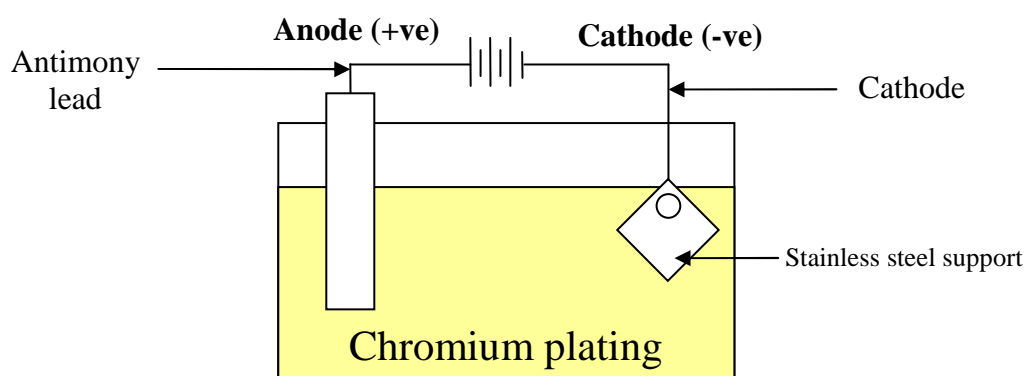
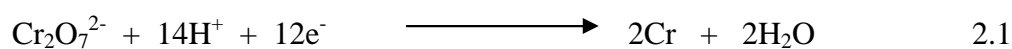


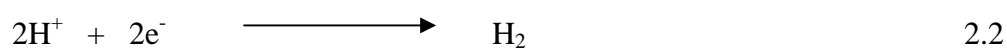
Figure 2.2 Scheme of Chromium electroplating.

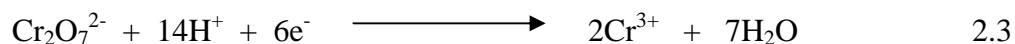
Now we fill the cell with a solution of a salt of the metal to be plated. It is theoretically possible to use a molten salt, and in rare cases that done, but most of the time the salt is simply dissolved in water and acid. The CrO_3 salt ionizes in water to Cr^{6+}

Deposition of chromium

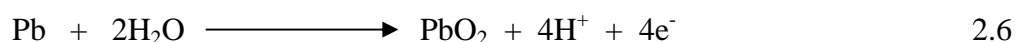


Evolution of hydrogen gas



Formation of chromium (III)

At the anode, liberation of oxygen is accompanied by the oxidation of trivalent of hexavalent chromium, i.e., the regeneration of chromic acid. The reaction was exhibited in equations 2.4 to 2.6.

Evolution of oxygen gas*Oxidation of chromium (III) to chromium (VI)**Formation of lead oxide***2.2.2 Electroless plating**

Electroless plating, also known as chemical or auto-catalytic plating, is a non-galvanic type of plating method that involves several simultaneous reactions in an aqueous solution, which occur without the use of external electrical power. Among other techniques, electroless deposition provides strong advantages such as uniformity of deposits even on very complex shapes, very simple equipment and low cost.

Electroless plating is possibly the simplest means of composite membrane fabrication, although support quality, surface activation methods, electroless plating procedures and bath chemistry influence membrane selectivity, permeability and Pd/Pd-alloy film stability. Therefore electroless plating will be discussed in the following three sections; surface activation, bath chemistry and electroless plating procedures.

2.2.3 Sputtering

This technique involves bombarding a target with energetic particles that cause surface atoms to be ejected and then deposited on a substrate close to the target. There are energy and momentum transfer between ions and atoms of the target. If the energy of target atoms overcomes the surface binding energy, the target atoms are ejected to form a film on a substrate. Figure 2.3 shows a schematic of a basic DC sputtering system.

The main advantage of this particular technique is that the evaporation rate is quite similar from one metal to another and therefore the technique is most suitable for the deposition of alloys. On the other hand, it is difficult to deposit a thin film using sputtering on certain supports such as a tube used widely in industries. Also, sputtering could not be used for coating the inside tube surface.

Reactive sputtering is the sputtering of an elemental target in the presence of a gas that with the target material to form a compound. In one sense all sputtering is reactive because there are always residual gases in the chamber that will react with the sputtered species.

Examples are when oxygen is injected into the chamber with the sputtering of aluminum to form aluminum oxide or when nitrogen is added with the sputtering of titanium to form titanium nitride.

The basic issue that must be faced during reactive sputtering is that the reactive gas combines with target material to form a compound.

The sputtering rate for the compound material that forms on the target is usually significantly less than the rate for the elemental target material. As the degree of target compound coverage increases, the deposition rate decreases.

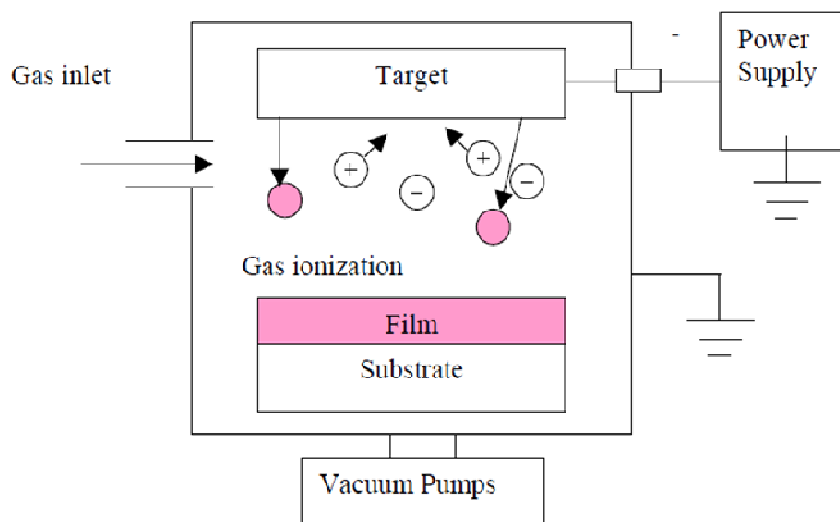


Figure 2.3 shows a schematic of a basic DC sputtering system.

2.3 Literature Review

2.3.1 Preparation of Cr_2O_3 and CrN thin films

Greeff, A.P. *et al* [15] have investigated the oxidation of the industrial FeCrMo steel. At high oxidation temperature the layer forms a duplex structure consisting of the Fe oxide at the gas/oxide interface and Cr oxide at the oxide/metal interface. The ratio between these oxides is temperature dependent. Below 400°C the oxide layer consists mainly of Fe_2O_3 and a small amount of Cr_2O_3 at the metal/oxide interface. Between 400°C and 600°C the oxide layer consists of mixture of FeO, Fe_2O_3 and Cr_2O_3 and above 600°C the layer consists mainly of Cr_2O_3 .

Sato *et al.* [16] investigated the oxidation behaviors of modified SUS316 (PNC316) and SUS316 stainless steels under the low oxygen partial pressure of 10^{-31} - 10^{-22} atm at 600 – 800°C . Oxygen uptake by these materials parabolically increased with time, and the kinetic rate constants depended on both oxygen partial pressure and

temperature. For the duplex layer formed under the low oxygen partial pressure, the inner layer consisted of such oxides as Cr_2O_3 and FeCr_2O_4 , while the outer layer consisted of non-oxidized α -Fe. Furthermore, oxidation along the grain boundaries was observed for samples oxidized for a long time. From the point of view of fuel cladding chemical interaction evaluation at high burn-up fuel for fast reactors, it is interesting that formation of non oxidized α -Fe was observed under the low oxygen partial pressure.

Lacoste *et al.* [17] reported that implantation of oxygen in stainless steel (15% Cr) via plasma-based ion implantation in a distributed ECR plasma reactor has been studied as functions of ion energy and dose. Due to the formation at the surface of dielectric films with optical index and thickness depending on the implantation time and pulse voltage (up to 44 kV), various colorations can be obtained. The experimental results demonstrate the feasibility of uniform processing, the possibility of reaching perfect control of the coloring through the dose and energy of implanted ions, and that the resulting coloration varies monotonically when increasing the dose and penetration depth of implanted oxygen. Characterization of the films by scanning electron microscopy and X-ray microanalysis shows that oxygen implantation results in strong surface oxidation, but without any significant degradation of the surface aspect. The thickness and composition profiles of the oxide layers determined using X-ray photoelectron spectroscopy, increases with ion energy and dose, but that the composition of the oxide layer resulting from. A uniform iron oxide layer (with a stoichiometry closed to Fe_2O_3), free from chromium, is formed in the near-surface region, while chromium segregates at the interface between the oxide layer and the bulk stainless steel to form chromium oxide Cr_2O_3 .

Sabioni *et al.* [18] prepared chromium protective layers were formed on many industrial alloys to prevent corrosion by oxidation. The role of such layers was to limit the inward diffusion of oxygen and the outward diffusion of cations. A number of chromium forming alloys contain iron as a major component, such as the stainless steels. To check if chromium is a barrier to the outward diffusion of iron in these alloys, iron diffusion in chromium was studied in both polycrystals and oxide films

formed by oxidation of Ni–30Cr alloy in the temperature range 700–1100 °C at an oxygen pressure equal to 10.4 atm. An iron film of about 80 nm thick was deposited on the chromium surface, and after the diffusing treatment, iron depth profiles were established by secondary ion mass spectrometry (SIMS). Two diffusion domains appear whatever the nature of the chromium material, polycrystals or films. In the first domain, using a solution of the Fick's second law for diffusion from a thick film, effective or bulk diffusion coefficients were determined.

Huntz *et al.* [19] reported that the oxidation behaviour of AISI 304 and AISI 439 stainless steels was studied at high temperatures, under various oxygen pressures and in the presence or not of water vapor. Thermogravimetric analyses were conducted in isothermal conditions from 850 to 950°C for 50 h and micro structural and chemical analyses of the oxide films grown by oxidation were performed by SEM and EDX. The oxide films were also analyzed by grazing X-ray diffraction and by X photoelectron spectroscopy (XPS). The AISI 439 steel has higher oxidation resistance than AISI 304, above 850°C, under high oxygen pressures. On the other hand, the AISI 304 steel has higher oxidation resistance under low oxygen pressures in the whole temperature range. In order to check whether the growth kinetics of Cr₂O₃ formed by the oxidation of stainless steels was controlled by oxygen or/and chromium diffusion through the oxide film.

Wang *et al.* [20] reported that metallic particles embedded in the oxide film play an important role in film's optical property. The result showed that metallic phases of Ag, Ti, and Pb can be formed in different oxide films under heating, X-ray photon, and electron radiation. The metallic phase separated from metal oxide film was investigated by X-ray photoelectron spectroscopy technique. Metal oxygen bond breaking and total energy reduction in the film. It is necessary to fully understand the formation mechanism of metallic particles so their shapes and distributions can be tailored to achieve the desired film's properties. Thermal activated metallic phase formation in first two cases can be explained by the bond breaking and reduction of total energy.

Earl *et al.* [21] studied the rates of oxidation of three heater alloys of nominal composition 80% nickel-20% chromium were studied over the temperature range of 500° to 950°C and at a pressure of 7.6 cm of Hg of oxygen, using the vacuum microbalance method. Temper color films were obtained for all oxidations below 850°C, while gray or gray-green films were obtained at temperatures of 850°C and higher. No evidence was found for scaling or cracking of the oxide from the alloys on cooling at temperatures of oxidation up to 950°C. The parabolic rate law was applied to the data. Reasonable agreement was found for temperatures above 650°C, while below this temperature the parabolic rate law constant varied with time. This time variation was explained in terms of composition changes in the oxide and growth of the oxide crystallite size. The classical theory of diffusion was used to interpret effect of temperature on rate of oxidation, and heats, entropies, and free energies of activation for the overall reaction were evaluated from the data.

Stefanov *et al.* [22] reported that the structure and composition of chromium oxide films formed on stainless steel by immersion in a chromium electrolyte have been studied by SEM and XPS. Cr₂O₃ crystallites in the range 30–150 nm are fully developed and cover the whole surface. The chemical compositions in the depth and the thickness of the oxide layer have been determined by XPS sputter profiles. The oxide film can be described within the framework of a double layer consisting of a thin outer hydrated layer and an inner layer of Cr₂O₃.

Shen *et al.* [23] reported that nanocrystalline chromium nitride (CrN) with the cubic rock-salt structure was synthesized by the arc discharge method in nitrogen gas (N₂). The product was characterized by X-ray diffraction (XRD) and transmission electron microscopy (TEM). It was found that the nitrogen gas pressure is a crucial factor for the synthesis of cubic CrN. At relatively low N₂ pressure, cubic CrN was formed. With the increase of N₂ pressure, hexagonal Cr₂N and metal Cr were gradually formed. It indicated that the formation of CrN is enhanced at a low nitrogen pressure environment, and the diffusion of nitrogen atoms into the Cr was lowered with the increase of N₂ pressure. They explain this experimental observation in terms of the evaporation rate of anode Cr and the ionization of nitrogen. In conclusion, they

have synthesized the cubic CrN nanocrystalline at a low nitrogen pressure of 5 kPa by the DC arc discharge method. The sizes of most CrN particles are less than 10 nm, with the increase of the nitrogen pressure, the amount of CrN decreases and the amount of Cr₂N and Cr increases. This indicates that the ability of nitridation falls, and the particle size also becomes much larger. The low-pressure synthesis of cubic CrN should be beneficial to improve nitridation of other transition metals such as, Co, Ta, Mo, and W.

2.3.2 Palladium membrane

Zhang, K. et al. [11] have reported the mesoporous yttria stabilized zirconia (YSZ) as intermediate layer for palladium membranes on porous metal supports. A thinner, gastight Pd layer can be formed on PSS support with the YSZ intermediate layer, resulting in a higher hydrogen permeance than Pd membranes on PSS support with the in situ oxidized metal oxide intermediate layer. At temperatures above 873 K, only the YSZ intermediate layer is effective in preventing intermetallic diffusion and gives a stable Pd membrane. At the elevated temperatures Pd membranes on PSS support with in situ oxidation layer suffer from a chemical and mechanical stability problem due to reduction of metal oxides in hydrogen atmosphere which results in intermetallic diffusion and possibly weakens the adhesion of the Pd layer on PSS support.

Ma, Y. H. *et al* [12] have reported the characterization of intermetallic diffusion barrier and alloy formation for Pd/Cu and Pd/Ag porous stainless steel composite membranes. The formation of the intermetallic diffusion barrier layer by the controlled in-situ oxidation method has been investigated by examining the morphological changes of the porous stainless steel support by SEM and EDS after oxidation in air. At oxidation temperatures lower than 600°C there might still be an oxide layer at the membrane-substrate interface although it was too thin to be detected and the alloy formation study showed that annealing at 600°C gave a uniform Pd/Cu-porous stainless steel (PSS) composite membrane, with no detectable presence of the elements from the PSS substrate.

Huang, Y. and Dittmeyer, R. [13] have reported the ceramic barrier for against intermetallic diffusion. The ceramic layer were coat by magnetron sputtering (MS-ZrO₂, thickness ~2 μm), atmospheric plasma spraying (APS-YSZ, thickness ~10-70 μm), and wet powder spraying (WPS-TiO₂, thickness ~40-60 μm), respectively. They differ considerably in terms of thickness, pore size, surface roughness, and open porosity. All three barriers as evidenced by tests in pure hydrogen at 600°C for up to 23 days. Among the three membrane types, Pd/WPS-TiO₂ demonstrated the best hydrogen permeance, i.e. 0.154 m³_{Nm}⁻²h⁻¹Pa^{-0.5}, as well as the best H₂/N₂-permselectivity, ~800, at 500°C. However, the highest hydrogen permeability, as determined from the permeance and the nominal thickness of the palladium membrane, was reached by Pd/APS-YSZ (1.6 m³_{Nm}⁻²h⁻¹Pa^{-0.5} at 500°C).

Shu, J.*et al* [24] have investigated the introduction of a titanium nitride for diffusion barrier and structurally stable composite Pd-Ag alloy membranes. To improve the structural stability of Pd-Ag alloy/SS membrane, an ultrathin intermediate layer of titanium nitride being 0.1 μm thick was introduced as a diffusion barrier between Pd-Ag and the SS substrate. The barrier only slightly modified the pore structure of the substrate as observed in the permeation measurements, but effectively separated the layer of Pd-Ag and substrate. The Auger electron depth profiling analysis indicated that the improved Pd-Ag/TiN/SS membranes were thermally stable at temperatures as high as 973 K.

Yepes, D *et al* [25] have proposed the different oxides for diffusion barriers in composite hydrogen permeable membranes. To improve the stability of the Pd-Ag alloy, two different intermediate layers of α-Fe₂O₃ and γ-Al₂O₃ oxides were employed as diffusion barrier. They also reported that the synthesized Pd-Ag/PSS membranes showed a good thermal stability and Pd-Ag/α-Fe₂O₃/PSS diffusion barrier exhibited an ideal selectivity higher than the Pd-Ag/γ-Al₂O₃ /PSS. However, the former membranes had two times higher hydrogen permeability.

Samingprai, S. *et al* [26] investigated chromium oxide intermetallic diffusion barrier for palladium membrane. Its hydrogen permeance was observed to decline at the temperature higher than 400°C. The chromium oxide layers at different thicknesses were then developed on oxPSS disks before palladium plating by controlled chromium electrodeposition followed by oxidation in air at 700°C. The result showed the hydrogen permeance of Pd/Cr₂O₃/oxPSS tube was observed to increase steadily with increasing temperature up to 500°C.

CHAPTER III

EXPERIMENTAL

3.1 Materials, equipment, and instruments

3.1.1 Materials

1. Stainless steel grade 316L, Mott Corporation
2. Palladium(II)chloride (PdCl_2), 99.9% , Alfa Aesar
3. Tetraamminepalladium (II) chloride monohydrate ($\text{Pd}(\text{NH}_3)_4\text{Cl}_2\cdot\text{H}_2\text{O}$) , 98% , Carlo Erba
4. Tin (II) chloride dehydrate ($\text{SnCl}_2\cdot 2\text{H}_2\text{O}$), 98% , Carlo Erba
5. Hydrazine anhydrous (N_2H_4), 99.5% , Aldrich
6. Disodium ethylenediaminetetraacetate (Na_2EDTA) , 99.5%, Carlo Erba
7. Quartz wool from Alltech
8. Helium gas, 99.999%, Bangkok Industrial Gas
9. Argon gas, 99.999%, Bangkok Industrial Gas
10. Hydrogen gas, 99.999%, Bangkok Industrial Gas
11. Nitrogen gas, 99.999%, Bangkok Industrial Gas
12. Sodium carbonate, Na_2CO_3 , Carlo Erba
13. Sodium hydroxide, NaOH , Carlo Erba
14. Trichloroethylene, C_2HCl_3 , Ajax Finechem
15. 2-propanol, $\text{C}_3\text{H}_7\text{OH}$, Carlo Erba
16. Acetone, from J.T Baker
17. Cr-Target for sputtering technique, Kurt J. Lesker
18. Detergent

3.1.2 Equipment

1. Furnace reactor, Lenton
2. Digital flow meter, Altech
3. Flow meter
4. Plasma sputtering chamber, in-house Photonic Technology Laboratory

3.1.3 Instruments

1. Scanning electron microscope (SEM), JEOL model JSM-5800LV with Energy Dispersive Spectrometer (EDS)
2. X-ray diffractometer, XRD, Bruker AXS, Germany Model D8 Advance

3.2 Experimental procedures

The experimental procedures were divided in to 3 steps:

1. Preparation of intermetallic diffusion barriers and palladium membrane
2. Intermetallic diffusion tests
3. Hydrogen permeation flux testing

3.2.1 Preparation of intermetallic diffusion barriers and palladium membrane

3.2.1.1 Preparation of supports

The 316L stainless steel (SS) disks and 316L porous stainless steel (PSS) were used for supports. Before plating, the surface of supports were cleaned to remove the foreign contaminates deposited such as oil, grease, dirt, and other. The

supports were cleaned with alkaline solution for electroplating and cleaned with commercial solvent for reactive sputtering.

3.2.1.1.1 Surface cleaning with alkaline solution.

The supports were cleaned in an ultrasonic bath with an alkaline solution at ~ 60°C for one hour and then thoroughly washed with deionized water and 2-propanol. The composition of alkaline solution is given in table 3.1. The supports were finally dried at 100°C for 3 hours.

Table 3.1 Composition of the alkaline solution

Compound	Amount
Na ₃ PO ₄ ·12H ₂ O	45 g/L
Na ₂ CO ₃	65 g/L
NaOH	45 g/L
Liquid detergent	5 mL

3.2.1.1.2 Surface cleaning with commercial solvent

Chromium and chromium nitride thin films were deposited on stainless steel substrates by magnetron sputtering technique. Prior the growth, the substrates were ultrasonically cleaned in trichloroethylene, acetone, 2-propanol and deionized water, respectively.

3.2.1.2 Preparation of Cr-based intermetallic diffusion barrier

Chromium oxide (Cr₂O₃) thin films were prepared by three techniques:

1. Thermal oxidation (TO)
2. Electroplating (EP)
3. Magnetron sputtering (MS)

Chromium nitride (CrN) thin film prepared by reactive d.c. magnetron sputtering (MS)

3.2.1.2.1 Thermal oxidation (TO) [15]

After cleaning, the disks were oxidized in a high temperature furnace at constant temperature under air. The heating and cooling rate were kept constant at 4°C/min. The supports used in this study were oxidized under normal atmosphere at several temperatures: 500, 600, 800°C and several oxidation times: 6 and 8 hours.

3.2.1.2.2 Electroplating (EP) [26]

The electroplating device setting was applied as shown in Figure 3.1. The chromium plating solution consisted of 250 g/L chromic acid and 1.25 g/L sulfuric acid as a catalyst in 200:1 ratio. The chromium plating was performed at room temperature with current density ~100-150 A/ft².

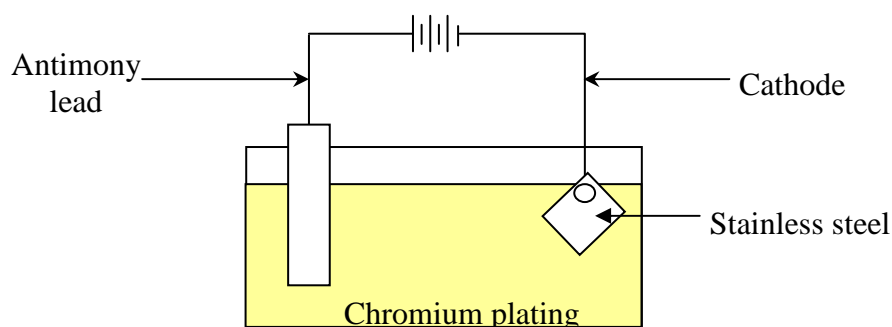


Figure 3.1 The chromium electroplating device.

Then the chromium oxide layer was generated by oxidizing in air at several temperatures: 500, 600, 800°C and several oxidation times: 6 and 8 hours.

3.2.1.2.3 Magnetron sputtering (MS) [27-28]

The concept of the sputtering process is that atoms of a target are bombarded by energetic ions. There are energy and momentum transfer between ions and atoms of the target. If the energy of target atoms overcomes the surface binding energy, the target atoms are ejected to form a film on a substrate. Figure 3.2 shows a schematic of a basic DC sputtering system.

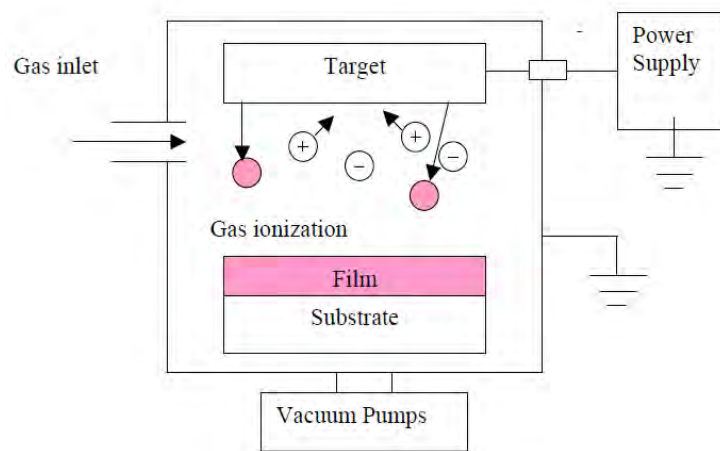


Figure 3.2 Schematic of a basic DC sputtering deposition system

1.) MS-Cr₂O₃

The chromium sputtering was prepared by sputtering from Cr target in argon atmosphere. The coating was deposited under a partial pressure of 2.5×10^{-3} bar. After that, it was oxidized at 600°C for 6 hours in air.

2.) MS-CrN

In the reactive sputtering process, chromium nitride thin films were produced from a pure chromium target in a mixing of argon and nitrogen pressure. Argon is inert gas while nitrogen is reactive gas. Sputtering condition, partial pressure of argon was constant of 6.1×10^{-3} bar and partial pressure of nitrogen was constant of 2.3×10^{-3} bar.

3.2.1.3 Electroless plating of palladium membranes

Electroless plating (ELP) was used to coat the intermetallic diffusion barrier with a continuous palladium layer. The general procedure for electroless plating was show in Figure 3.3.

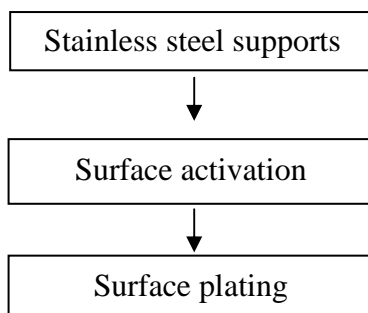


Figure 3.3 Scheme of general procedure for palladium plating

3.2.1.3.1 Surface activation

The supports (with intermetallic diffusion barrier) were activated before electroless plating to seed the surface layer with nuclei of palladium. The activation process consisted of successive immersion of the supports in the tin chloride (SnCl_2) solution followed by palladium chloride (PdCl_2) solution with rinsing in deionized water between these baths, at room temperature. The typical composition of the activation bath is presented in table 3.2 [29]. The sequence of surface activation steps were show in Figure 3.4. The activation process was continued until the surface became grayish brown.

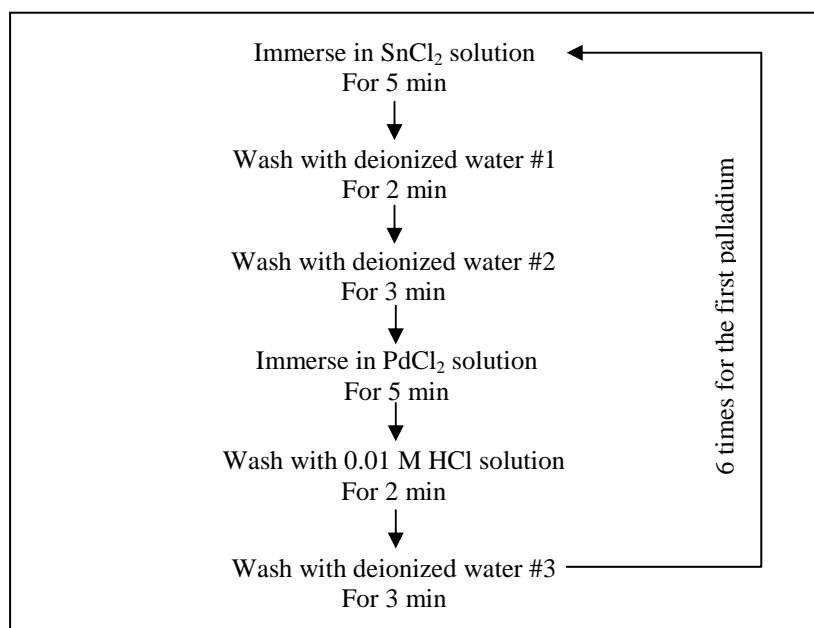


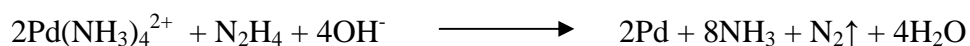
Figure 3.4 Scheme the procedure for surface activation steps.

Table 3.2 Chemical composition of activation bath

Chemical	Amount
SnCl ₂	1.0 g/L
HCl (37%)	1.0 mL/L
PdCl ₂	0.1 g/L
HCl (37%)	1.0 mL/L

3.2.1.3.2 Palladium electroless plating

The plating solution was prepared by mixing the first three compounds given in Table 1.3. The palladium membrane was deposited at 60°C for 90 min. The plating solution was renewed every 90 min. The plating reaction is



After deposition was complete the membrane was allowed to cool down at room temperature in deionized water and dried at 100°C for 3 hours.

Table 3.3 The composition of electroless palladium plating solution

Chemical	Amount
Tetraaminepalladium (II) chloride, Pd(NH ₃) ₄ Cl ₂ ·H ₂ O	4.0 g/L
Ammonia solution, NH ₄ OH (28%)	198 mL/L
Disodium ethylenediaminetetraacetate, Na ₂ EDTA	40.1 g/L
Hydrazine anhydrous, N ₂ H ₄ (1M)	5.6-7.6 mL/L

3.2.2. Intermetallic diffusion tests

Intermetallic diffusion tests were done on four Pd membranes. First, disk of Pd membranes were placed into a reactor a heated under helium flow (~20 ml.min⁻¹) at a ramp of 4°C min⁻¹. When the temperature reached 400°C, switch to pure hydrogen with a flow rate of ~20 ml.min⁻¹ for 24 hours, the membrane was cooled to 400°C, and hydrogen was replaced with helium before further cooling down to room

temperature. The supports used in this study were tests at several temperatures: 500, 600, 800°C. The sample was characterized by SEM-EDS.

3.2.3 Hydrogen permeation flux testing

Hydrogen permeation was performed in a permeator cell as shown in Figure 3.5. The open end of the membrane was sealed to the permeator wall with graphite gasket. The pressure of feed gas was monitored by a pressure gauge. The gas permeation rate (the volumetric flow rate) was measured in the permeate side at atmospheric pressure and room temperature. The temperature of the permeator was varied from 350-500°C. Prior to the hydrogen permeation flux testing, the dense palladium membrane disk was heated in helium at the rate about 4°C/min before subjecting to hydrogen. The gas permeation rates were measured using two bubble flow meters at room temperature and pressure.

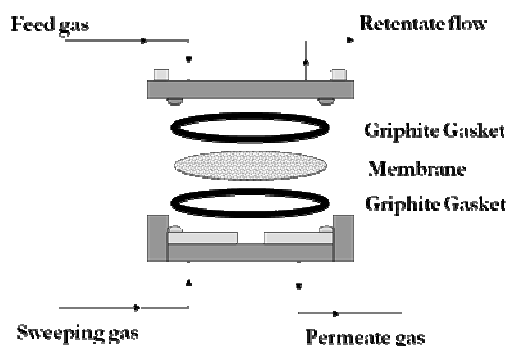


Figure 3.5 Schematic of the permeator cell

CHAPTER IV

RESULTS AND DISCUSSION

4.1 Preparation of intermetallic diffusion barriers and Pd membrane

4.1.1 Characterization of support

Several studies was used 316L porous stainless steel (PSS) support with average pore size $\sim 0.1\text{-}0.5\ \mu\text{m}$ for Pd membranes reactor [30-32]. It had several advantages comparing to other supported materials; high resistance to corrosion, tougher and stronger than other materials. The 316L stainless steel (SS) disk and 316L PSS disk were chosen as a support in this study. In order to compare result, both supports have a thickness of 1 mm. The SS and PSS support were used for intermetallic diffusion barrier test and hydrogen permeation flux test, respectively. The SS support was cut into $1\times 1\ \text{cm}^2$. The PSS support has the average pore size of $0.2\ \mu\text{m}$.

Table 4.1 Elemental compositions of the SS and PSS supports

Elements	Atomic %	
	SS support	PSS support
Mn	1.44	-
Cr	16.70	20.48
Fe	70.37	67.90
Ni	9.85	11.62
Mo	1.68	-
Totals	100	100

The elemental of the both supported was determined with the EDS spot scan technique. The elemental compositions given in Table 4.1 approximate ~ 16.70 and 20.48 atomic % of Cr for SS and PSS support, respectively.

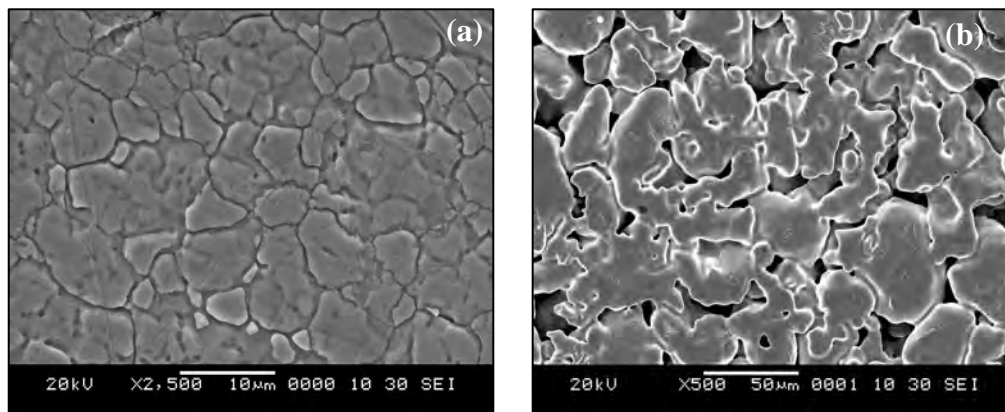


Figure 4.1 SEM micrographs of stainless steel (SS) support (a), and (b) of porous stainless steel (PSS) support

SEM micrographs showing the surface morphology of SS and PSS supports are illustrated in Figure 4.1. Figure 4.1 (a) shows that the grains on the surface of SS support and Figure 4.1 (b) show the pore size distribution of PSS support, much larger pores could be observed on the surface.

4.1.2 Preparation of Cr-based intermetallic diffusion barriers

In this study chromium oxide and chromium nitride were constructed to be the diffusion barriers on the stainless steel support. There were three different methods to prepare chromium oxide and one method for chromium nitride on SS disks, $1 \times 1 \text{ cm}^2$

4.1.2.1 Chromium oxide by thermal oxidation

In-situ thermal oxidation in air was employed to introduce an oxide layer on the surface of SS disks. The oxidation processes were oxidizing in air at 500-700°C for 6-8 hours. After heating in air, the color of SS disks changed from silver to red-purple when oxidized at 500°C, to green when oxidized at 600°C and to dark-green when oxidized at 700°C. The resulted oxidized SS disks were determined by XRD spectroscopy and SEM-EDS.

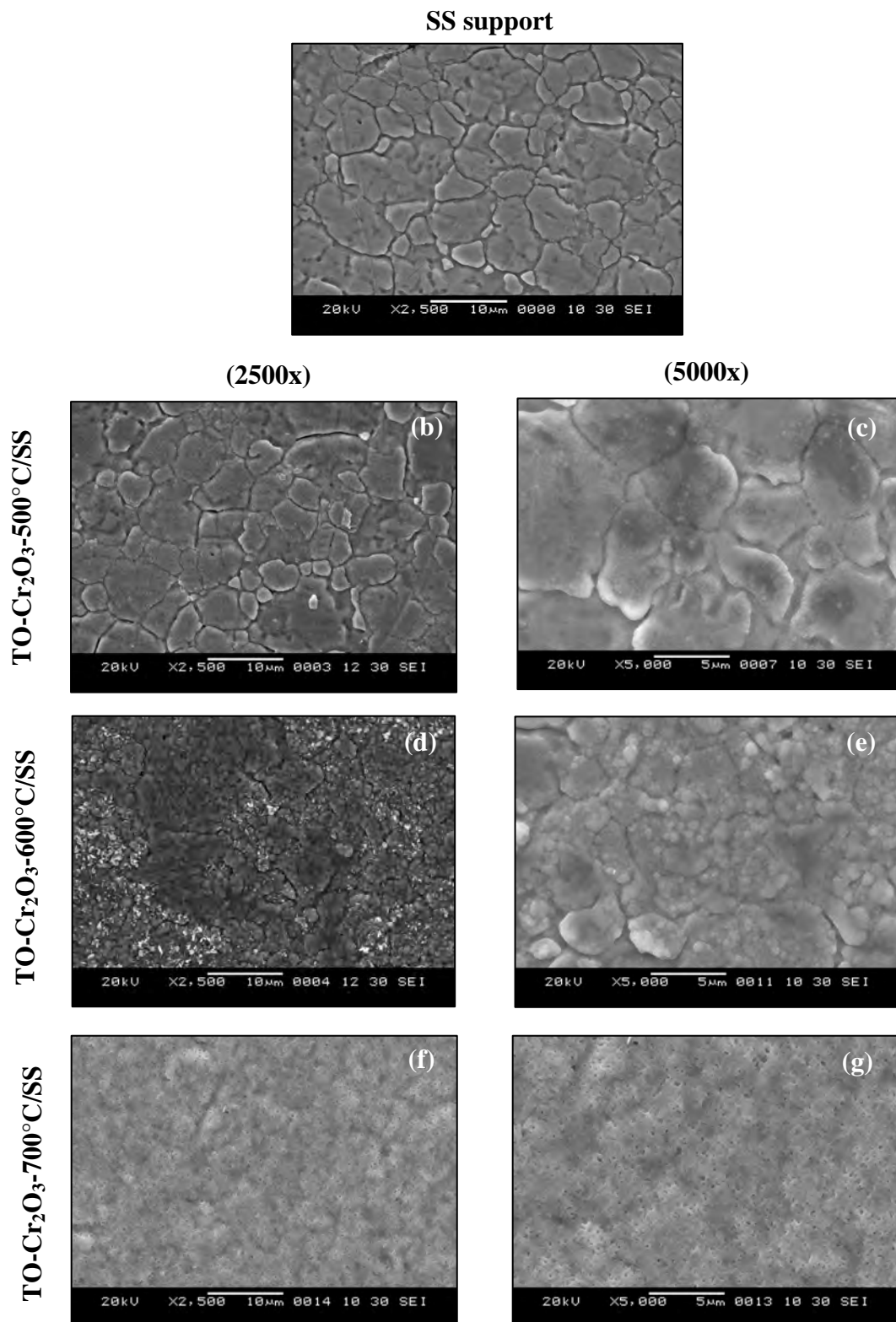


Figure 4.2 SEM micrographs of the surface of SS disks before (a) and after oxidation in air at 500°C (b, c), 600°C (d, e), 700°C (f, g) for 6 hours.

Figure 4.2 shows the SEM micrographs of the surface of SS disks before and after oxidation in air at various temperatures for 6 hours. It can be seen that SS disks surface of Figure 4.2 (a), unoxidized SS disk, and Figure 4.2 (b, c), oxidized at 500°C, looked smooth and similar, whereas the surfaces of Figure 4.2 (d, e) and Figure 4.2 (f, g), oxidized at 600°C and 700°C respectively, were much rougher. For Figure 4.2 (f, g), the surface was very crumbly and the roughness seemed to increase substantially compare to the SS disk unoxidized.

The oxidation process was followed by XRD. The crystallographic structures of Fe_2O_3 , Cr_2O_3 and all Fe-Cr mixed oxides were very similar. The XRD pattern of Fe_2O_3 oxide has distinctive reflections at $2\theta \approx 33.152, 35.611, 49.479, 54.089, 62.449$ and 63.994° . The XRD pattern of Cr_2O_3 oxide has the same distinctive reflections with a slight shift to right: $33.597, 36.196, 50.219, 54.853, 63.448$ and 65.108° . The XRD reflections of all Fe-Cr mixed oxide lie between the XRD reflections of Fe_2O_3 and Cr_2O_3 with peak positions depending on the Fe/(Fe+Cr) ratio.

The XRD patterns of the SS disk before and after oxidized at varied temperatures in 6 hours (a) and 8 hours (b), as shown in Figure 4.3, displayed that no peaks position depending on SS disk at the oxidation temperature lower than 600°C. Both the SS disks oxidized at 600 and 700°C in 6 hours (a) and 8 hours (b) revealed the present formation of Cr_2O_3 . Moreover, the SS disks oxidized at 700°C observer formation of Fe_2O_3 at the surface of the sample in agreement with Fe_2O_3 - Cr_2O_3 structure found using EDS technique.

Among these metal oxides, Cr_2O_3 thin film can inhibit the intermetallic diffusion due to the Tamman temperature of Cr_2O_3 which is much higher than the working temperature of the palladium membrane.

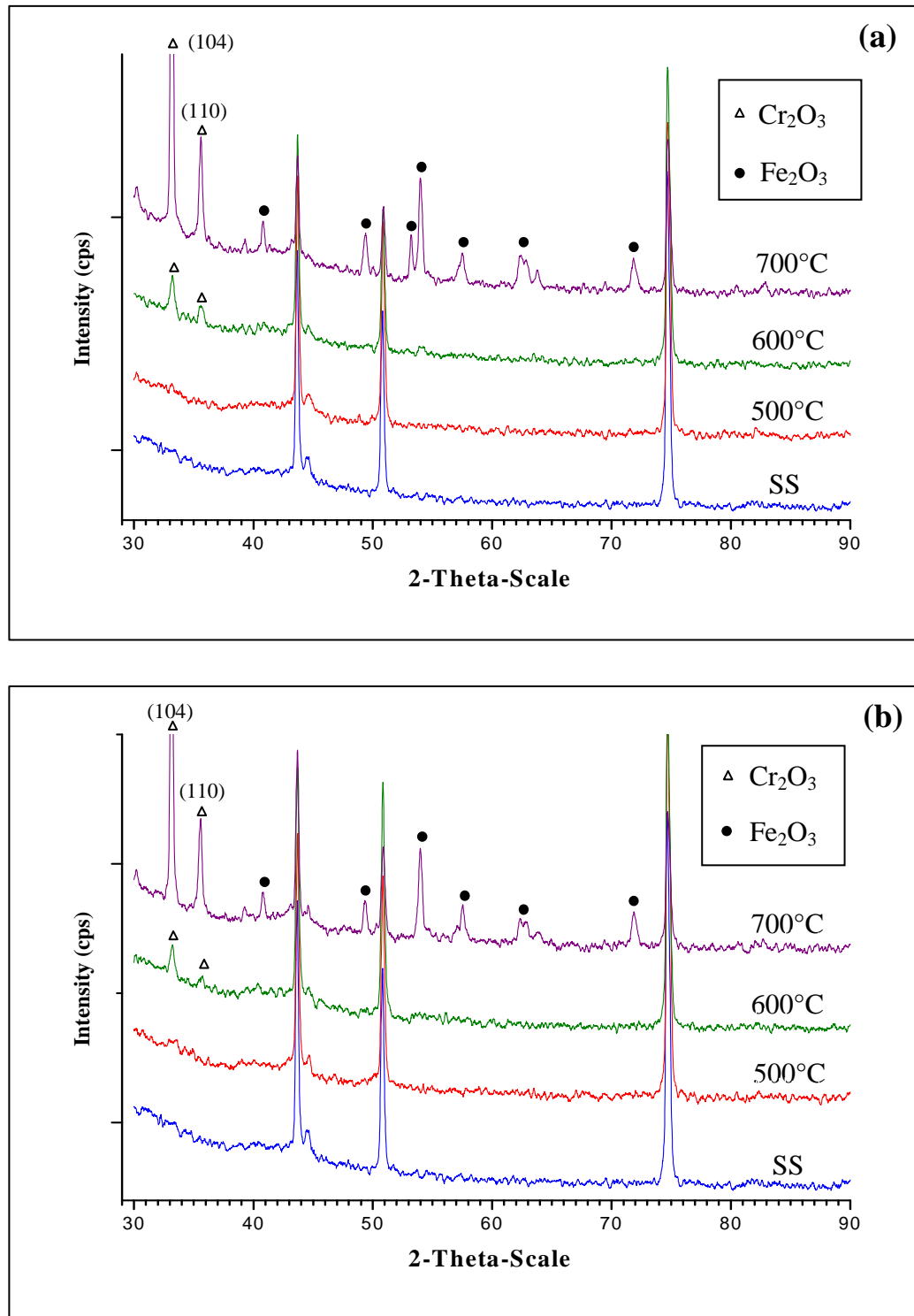


Figure 4.3 X-ray diffraction patterns of the SS disks and SS disks after oxidized in 6 hours (a) and 8 hours (b).

Figure 4.4 shows the EDS spectra on the surface of SS disk oxidized at 600 and 700°C for 6 hours. The oxygen peak observed confirms the formation of an oxide layer on the support. It was also observed that the amount of oxygen on the SS disk was increased with higher oxidation temperatures in contrast with amount of chromium on the surface decrease.

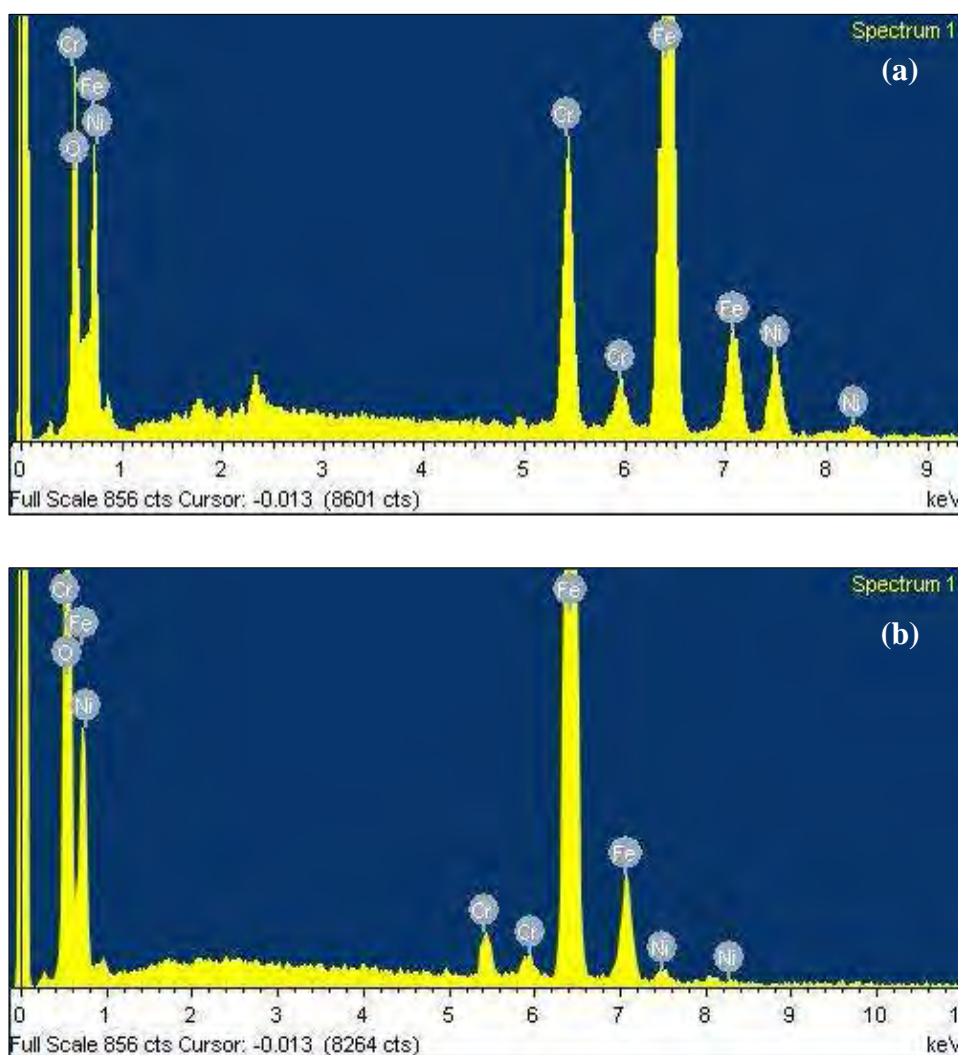


Figure 4.4 EDS spectra of SS disks after oxidized at 600 (a) and 700°C (b) for 6

Therefore it is the most desirable oxide phase for use as a barrier layer to the intermetallic diffuse, EDS spot scan analysis was performed. The ratio of atomic Fe to atomic Cr on the surface of the supports is shown in Figure 4.5. The ratio

remained almost constant and essentially the same as the unoxidized sample for the samples oxidized at 500°C and 600°C whereas it increased dramatically for the support oxidized at 700°C indicating a Fe-rich oxide on the outermost layer.

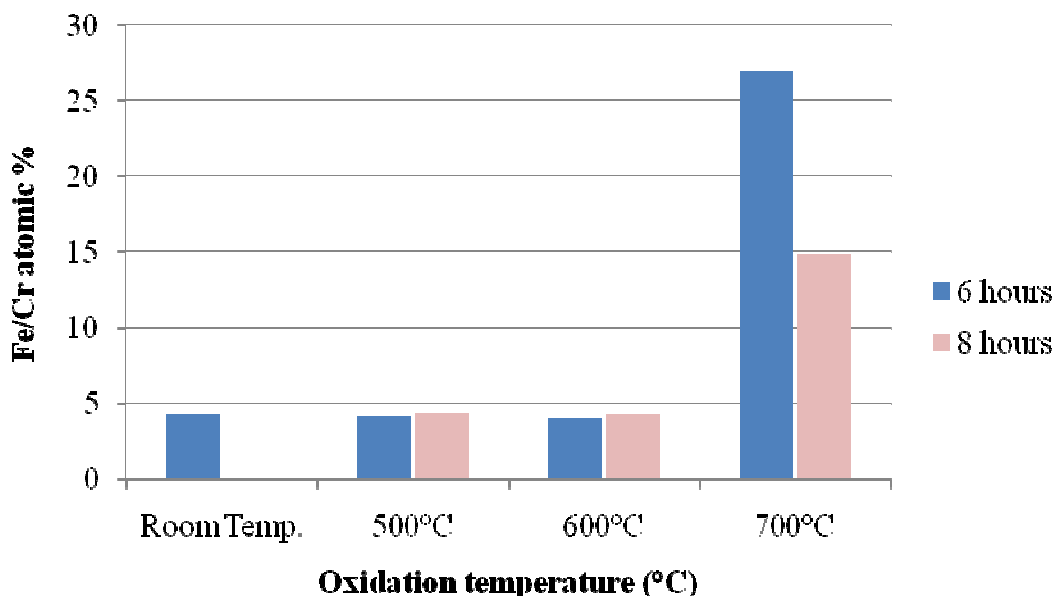


Figure 4.5 Ratio of Fe/Cr obtained from EDS spot scan analysis of the surface of the oxidized SS disks.

The ability of the oxide layer to minimize intermetallic diffusion is a function of its thickness and more importantly, of the nature of the oxide at the surface of the support. As discussed by Guazzone et al [33], oxidizing at 600°C in stagnant air led to a thin (0.5-0.8 μm) oxide layer consisted of stable chromium oxide layer (0.1-0.2 μm) and an iron oxide layer on top (0.4-0.6 μm).

4.1.2.2 Chromium oxide by electroplating (EP- Cr_2O_3)

Chromium (Cr) was coated on the SS disk by electroplating (EP) method and the oxidation to form Cr_2O_3 using the same condition as the thermal oxidation method. After heating in air, the color was changed from gray to green. The Cr thin film thickness was calculated as follows:

$$Cr \text{ thickness } (\mu\text{m}) = \left[\frac{(\text{plated disk weigh} - \text{initial disk weigh})}{(\text{disk surface area} \times \text{chromium density})} \right] \times 10^4$$

Where density of chromium = 7.14 g/ml.

The reliability of the gravimetrically method for determining the Cr layer thickness was assessed with their SEM micrographs.

Table 4.2 Thickness of Cr thin films at different deposition time

Disk number	Deposition times (min)	Disk weight (g)		Thickness (μm)	
		Before plating	After Plating	Determine	SEM
1	1	0.7354	0.7375	1.22	3.23
2	2	0.6979	0.7031	3.03	5.66
3	3	0.7268	0.7368	5.83	7.41

Table 4.2 show the deposition rate of Cr film on SS supports. The Cr deposition time increased with deposited time. Then the Cr_2O_3 layer was generated by oxidizing in air. The Cr_2O_3 formation which was confirms by XRD and EDS.

Figure 4.6 shows XRD patterns of Cr thin films after oxidizing in air, displayed that no Cr_2O_3 formation could be detected at the oxidation temperature lower than 600°C . The increase in intensity of Cr_2O_3 peaks was observed at higher oxidation temperature and appeared that Fe_2O_3 peaks at the oxidation temperature 700°C . Although Cr_2O_3 from in oxidation time for 6 hours seemed to be a little better than 8 hours.

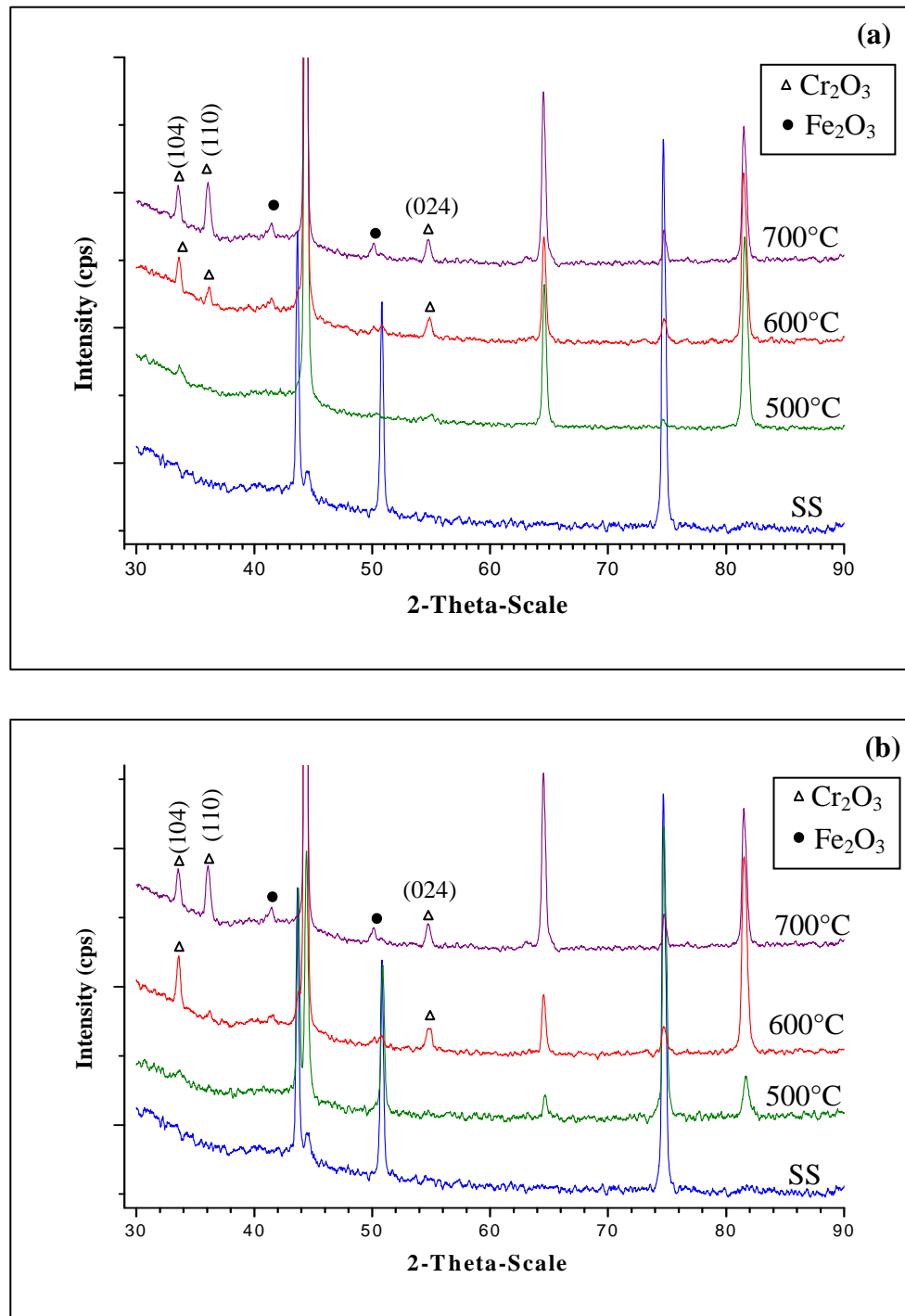


Figure 4.6 X-ray diffraction patterns of the Cr thin film on SS disks after oxidized in 6 hours (a) and 8 hours (b).

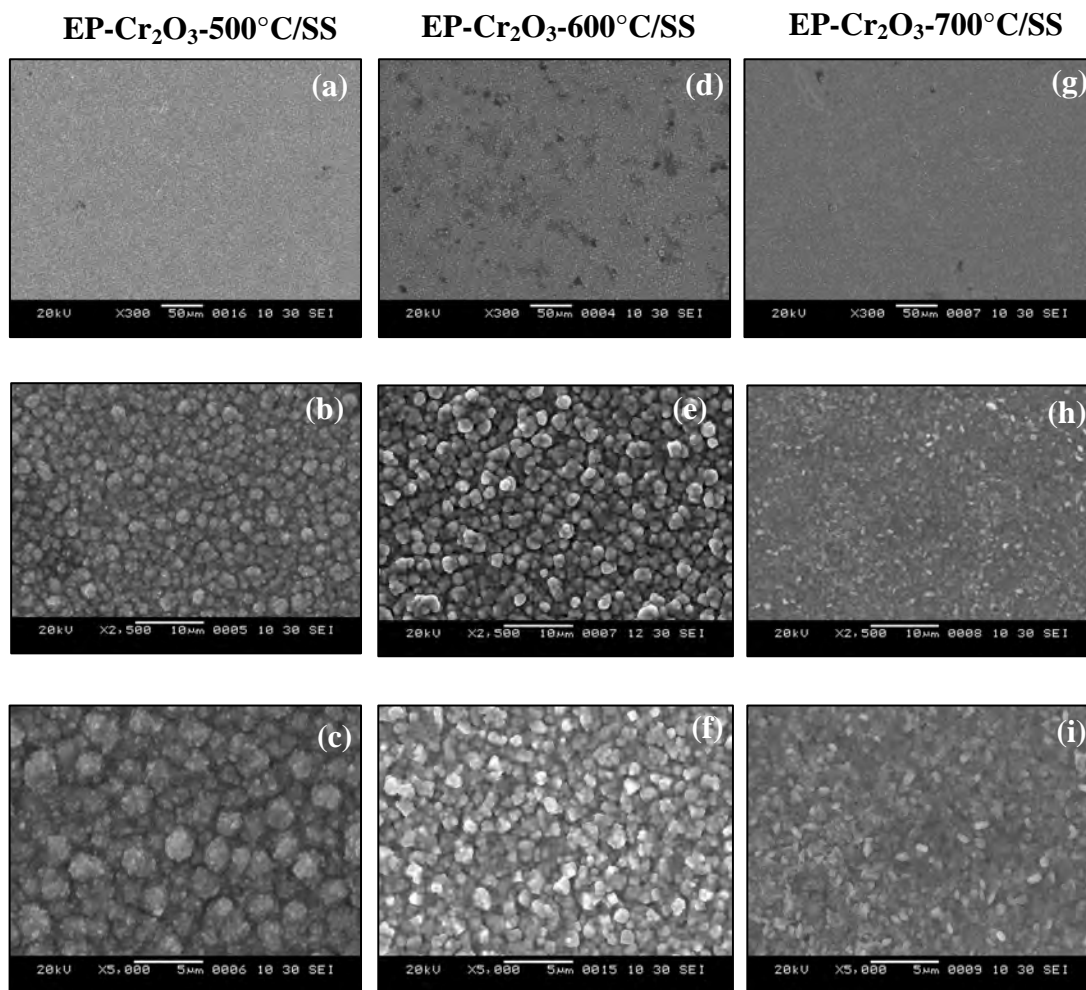


Figure 4.7 SEM micrographs surface of Cr-thin film by EP method after oxidation 500°C (a, b, c), 600°C (d, e, f), 700°C (g, h, i) for 6 hours.

Figure 4.7 shows the SEM micrographs of the surface of Cr-thin film by electroplating method after oxidizing at 500-700°C for 6 hours. It can be seen that surface of was roughen and the Cr_2O_3 particles were decrease with higher oxidation temperature.

The Cr_2O_3 thin film was successfully deposited on the SS disk by electroplating method and oxidation in air. The results of the XRD patterns and EDS spectrum, it was found that suitable oxidation temperature was therefore considered to be at 600°C for 6 hours. It was called that EP- Cr_2O_3 . Furthermore, the effect of chromium layer thickness was investigated. The chromium thickness was varied from 2 - 6 μm .

4.1.2.3 Chromium oxide by magnetron sputtering (MS-Cr₂O₃)

The Cr was deposited by magnetron sputtering, using a pure Cr target in an argon atmosphere. The deposition parameters that used in the process are summarized in Table 4.3. A series of Cr depositions were done to on the SS disks for 15, 30 and 45 min and the results in a thickness of 1, 1.5 and 2 μm , respectively. The deposition rate was increases with increasing deposition time. Then, the oxidized at 500- 700°C for 6 hours in air to evaluate the Cr₂O₃ formation.

Table 4.3 Experimental condition for deposition of Cr coating

Bias voltage (V)	0
Growth temperature (°C)	RT
Base pressure (mbar)	6.5×10^{-6}
Total pressure (mbar)	3.3×10^{-3}
The partial pressure of Ar (mbar)	2.5×10^{-3}
The Ar flow (sccm)	4.1
Deposition time (min)	15, 30, and 45
The distance between the target and substrate (cm)	7

Figure 4.8 shows the SEM micrographs of the Cr thin films surface after oxidation. It can be seen that surface was small Cr cluster than the surface of electroplating method. The XRD patterns of the Cr thin films before and after oxidation at 500-700°C for 6 hours in air are shown in Figure 4.9. The XRD patterns displayed as same as the electroplating method, no Cr₂O₃ peaks at the oxidation temperature lower than 600°C and appeared that Fe₂O₃ peaks at the oxidation temperature 700°C. The suitable oxidation temperature was therefore considered to be at 600°C.

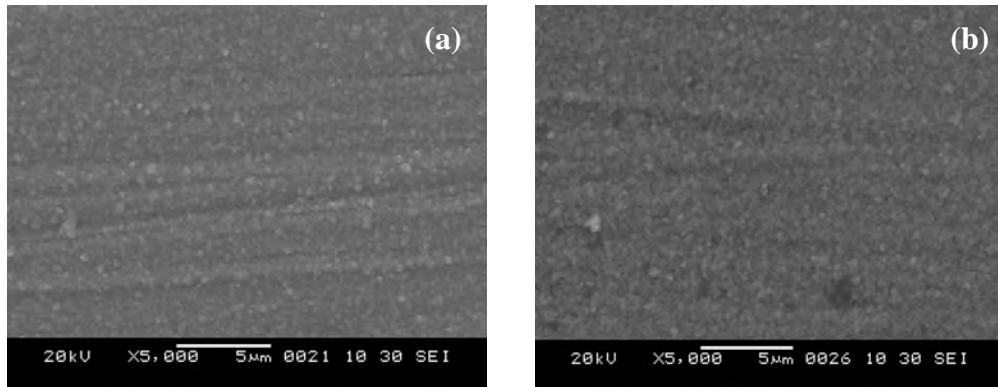


Figure 4.8 SEM micrograph surfaces of Cr-thin film by MS method after oxidation 600°C (a), 700°C (b) for 6 hr

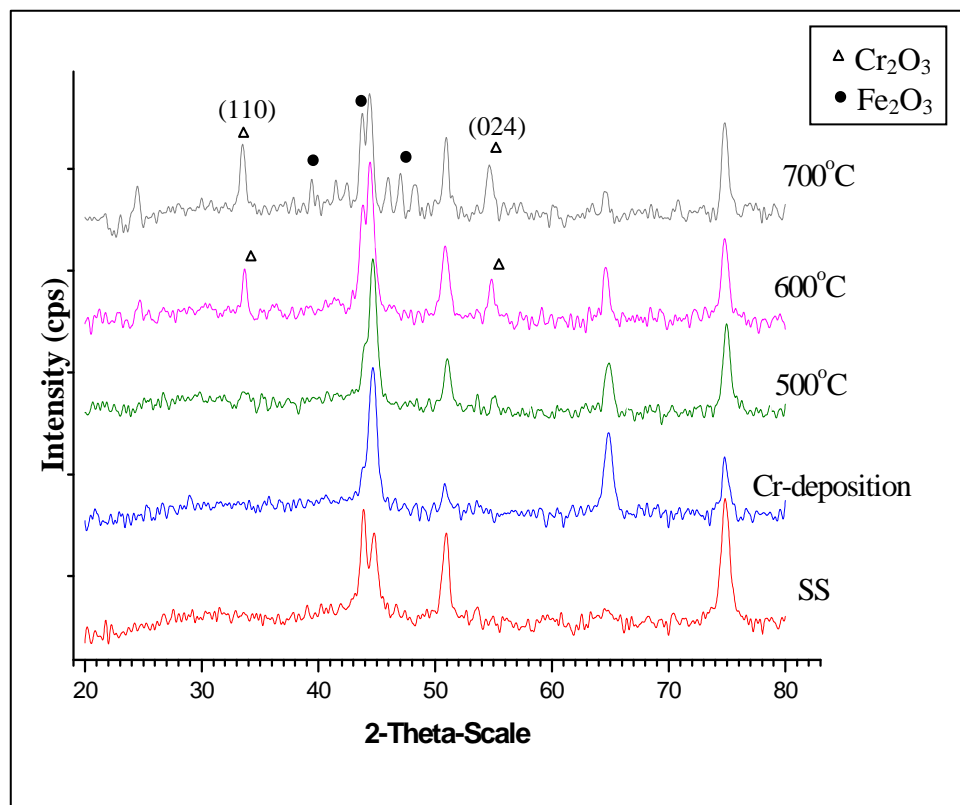


Figure 4.9 The X-ray diffraction patterns of the Cr thin film on SS disks after oxidized in 6 hours.

4.1.2.4 Chromium nitride by magnetron sputtering (MS-CrN)

In the reactive sputtering process, chromium nitride thin films were produced from a pure chromium target in a mixing of argon and nitrogen pressure [34]. Sputtering condition is listed in Table 4.4. The sputtering times were 30 and 60 min for 2 and 3 μm , respectively. The sputtering rate for the CrN thin film is less than the rate for Cr thin film. As the degree of target compound coverage increases, the deposition rate decreases.

Tabel.4.4 Experimental condition for deposition of CrN coating

Bias voltage (V)	0 V
Growth temperature ($^{\circ}\text{C}$)	RT
The partial pressure of N_2 (mbar)	6.1×10^{-4}
The partial pressure of Ar (mbar)	2.3×10^{-4}
The Ar flow (sccm)	4.0
The nitrogen flow (sccm)	2.4
Deposition time (min)	30 and 60
The distance between the target and substrate (cm)	7

Chemical composition of the chromium nitride coatings was investigated by use of EDS. The content of nitrogen and chromium were 53.95 and 46.08 atomic %. The requirement composition of nitrogen in the film is in the range between 45 and 55 %. This composition makes the film be stoichiometric.

The XRD pattern of the CrN thin film was shown in the Figure 4.10. The CrN (111), (200) reflections can be observed. This result of the XRD and EDS spot scan could confirm that the stoichiometrical CrN thin films exhibit on SS disk.

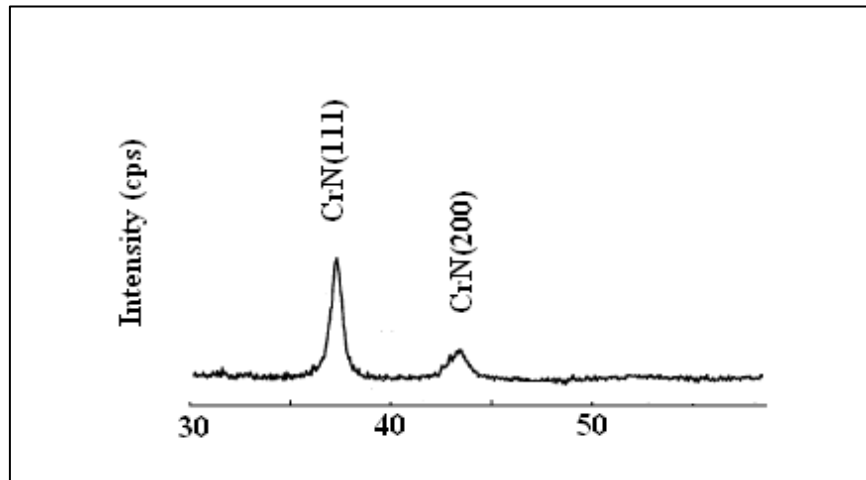


Figure 4.10 X-ray diffraction patterns of the CrN thin film

Figure 4.11 shows SEM micrograph of surface of the CrN thin film on SS disk. After being deposited of CrN thin film, SS disk demonstrated as same as before deposited of CrN thin film. It could not change morphology of SS disk surface because of it too thin and had color as same as to SS disk.

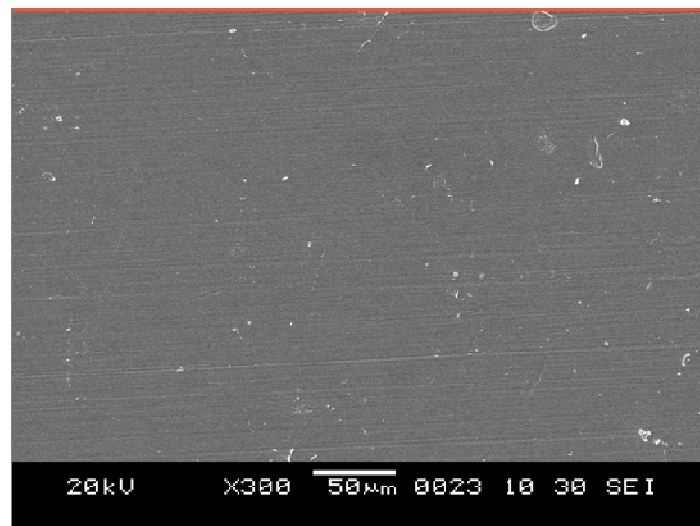


Figure 4.11 SEM micrograph surfaces of CrN thin film by reactive magnetron sputtering method

4.1.3 Electroless plating of palladium membranes

The electroless plating technique was used in preparing the palladium membrane on the stainless steel supported. It started with surface cleaning with alkali solution, prepared of intermetallic diffusion barrier, surface activation by using $\text{SnCl}_2/\text{PdCl}_2$ solution, and palladium plating by palladium complex solution. The thickness of the palladium layer was calculated as follows:

$$\text{Pd thickness } (\mu\text{m}) = \left[\frac{(\text{plated disk weigh} - \text{initial disk weigh})}{(\text{disk surface area} \times \text{palladium density})} \right] \times 10^4$$

Where density of palladium = 12.02 g/ml.

The reliability of the gravimetrically method for determining the palladium layer thickness was assessed with their SEM micrographs. The morphology of the palladium deposition film was observed by SEM micrograph. As seen from the SEM micrographs in Figure.4.12, the top surface became smooth on SS disk.

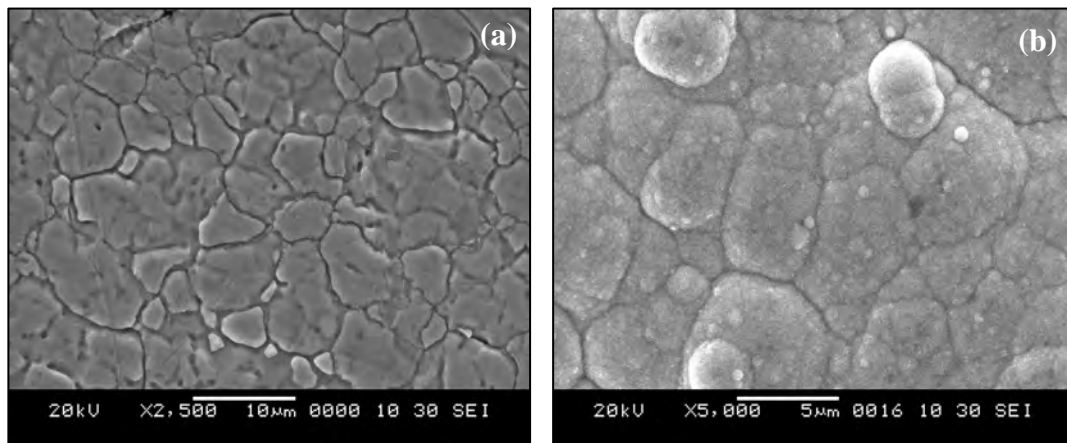


Figure 4.12 SEM micrographs of SS disk (a) and palladium layer on SS disk (b)

After the Pd deposited, the helium flux was used to check if the Pd layer was dense. The membrane is deemed 'dense' when there was no He flux at room temperature under a pressure difference of 1 atm for the hydrogen flux test.

4.2 Intermetallic diffusion tests

The fundamental understandings of the efficacies in preventing intermetallic diffusion of the intermetallic diffusion barrier were assessed by hydrogen expose the palladium membrane with either of the barriers at 400, 500, and 600°C for 24 hours. SEM-EDS line scan was applied to analyze the elemental content of the palladium layer after hydrogen exposure. In Figure 4.15 (a) shows the line scans of Pd membrane in fresh state were performed starting from the inner of the SS disk and ending at the outer rim of the Pd layer and it should be noted that the spatial resolutions for EDS line scan (b) was in the range of $\pm 0.5 \mu\text{m}$ due to the beam width of the electron beam which was about $3 \mu\text{m}$.

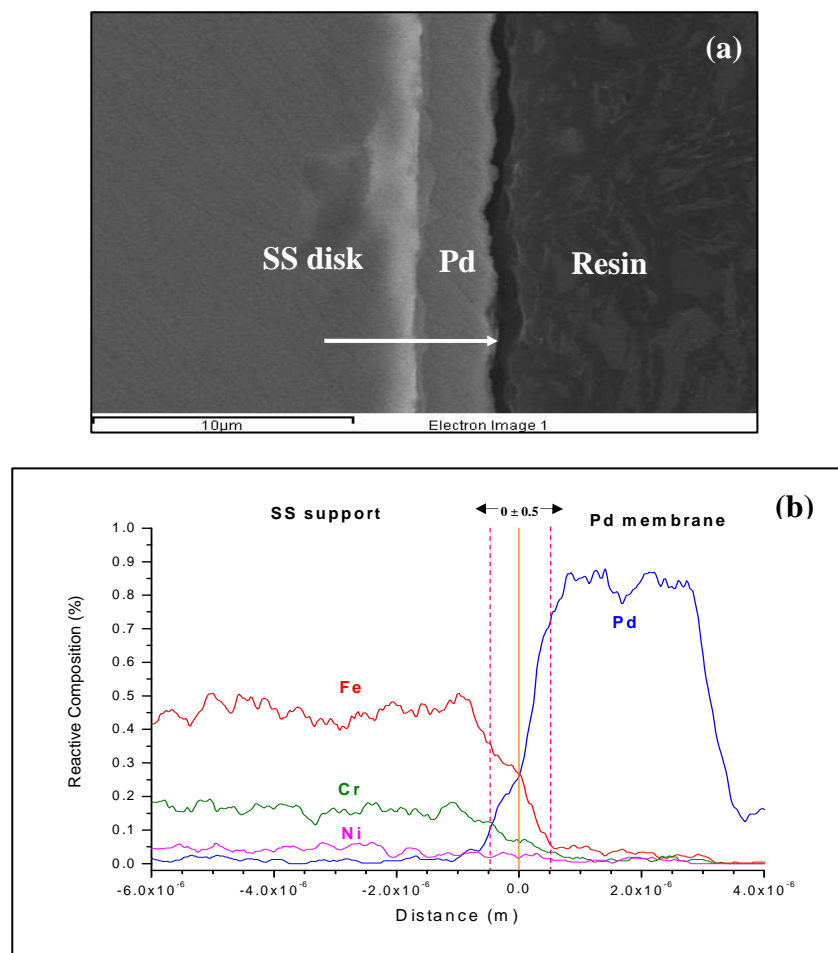


Figure 4.13 SEM micrograph (a) and EDS line scan (b) of Pd membrane in fresh state

The prepared conditions of the intermetallic diffusion barriers used in this study are summarized in Table 4.5.

Table 4.5 The prepared conditions of the intermetallic diffusion barriers

Disk no.	Synthesis type	Thickness of barrier (μm)	Hydrogen exposure temperature ($^{\circ}\text{C}$)		
			400	500	600
# 01	-	-	√		
# 02				√	
# 03					√
# 04	Cr_2O_3 by TO method at 600°C for 6 hours in air	too thin (nm)	√		
# 05				√	
# 06					√
# 07	Cr_2O_3 by EP method 1 min and oxidation at 600°C for 6 hours in air	4-6	√		
# 08				√	
# 09					√
# 10	Cr_2O_3 by EP method 0.5 min and oxidation at 600°C for 6 hours in air	2-3	√		
# 11				√	
# 12					√
# 13	Cr_2O_3 by MS method 45 min and oxidation at 600°C for 6 hours in air	2	√		
# 14				√	
# 15					√
# 16	Cr_2O_3 by MS method 15 min and oxidation at 600°C for 6 hours in air	1	√		
# 17				√	
# 18					√
# 19	CrN by reactive MS method for 60 min	3	√		
# 20				√	
# 21					√
# 22	CrN by reactive MS method for 30 min	2	√		
# 23				√	
# 24					√

Pd/SS non barrier (disk #03) was shown in Figure 4.14. After hydrogen exposure at 600°C for 24 hours, it was found that the metal of SS disk (Fe, Cr, and Ni) diffuse into the palladium layer. Among three metals, Fe was always found to be the highest content in palladium layer. The diffusion coefficient of Fe in Pd is equal to $0.81 \cdot \exp(-260000/RT) \text{ cm}^2\text{s}^{-1}$. On the other hand, Pd/SS non barrier (disk #01 and #02) were detected of elemental in SS disk in Pd layer as same as disk #03. The elemental diffusion rate increased with the hydrogen exposure temperatures increasing.

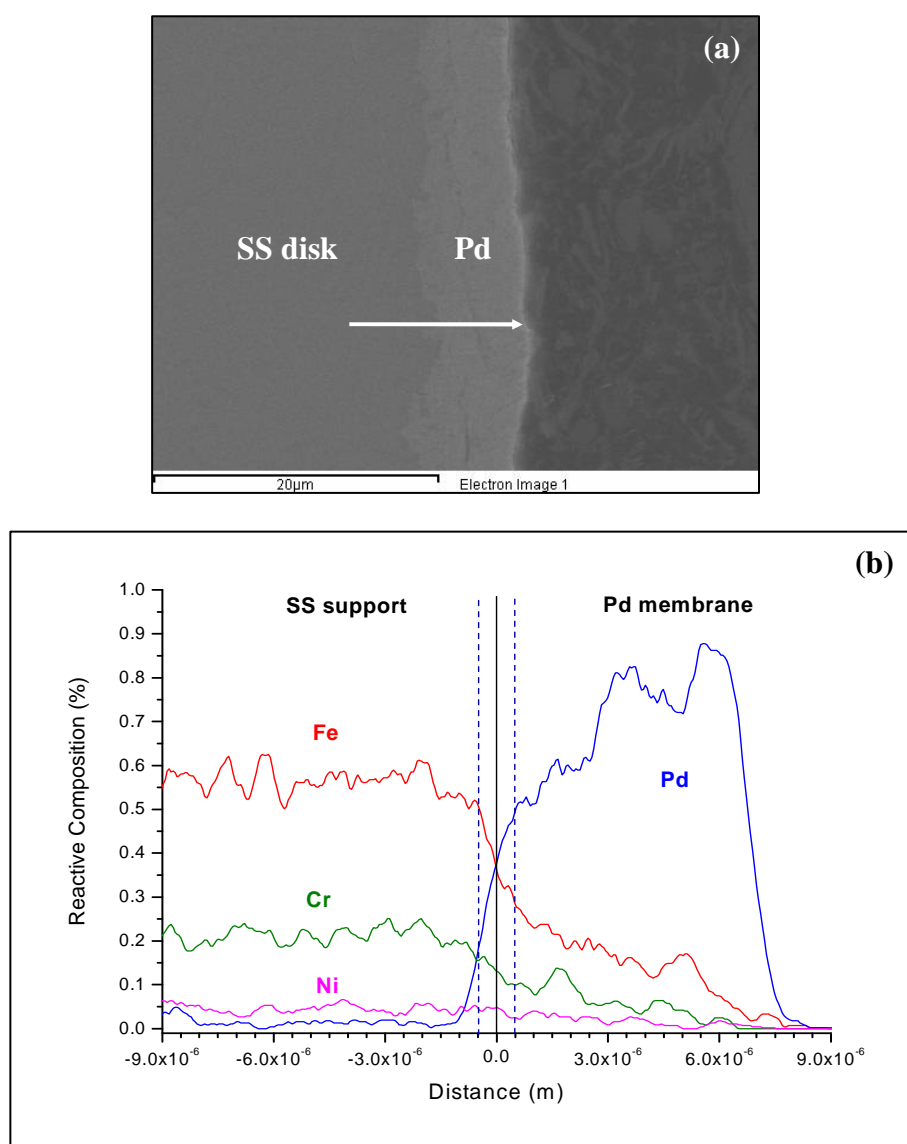


Figure 4.14 SEM micrograph (a) and EDS line scans (b) of Pd/PSS non barrier (disk #03) after hydrogen exposure at 600°C for 24 hours.

For the barrier of Pd/TO-Cr₂O₃/SS (disks #04 - #06) could not be detected by the EDS line scan, the oxide was probably in the nm scale. This was consistent with Shibagaki *et al.* [35], who using μ AES, reported a 16 nm thick oxide layer on 316L stainless steel after oxidation at 427°C in air. The existence of an oxide layer and the growth of oxide layer with increasing oxidation temperatures have been reported by many authors. For high oxidation temperatures, the thick oxide layer consisted of a Fe-rich oxide layer on top followed by a mixed Cr and Fe oxide layer [35-36].

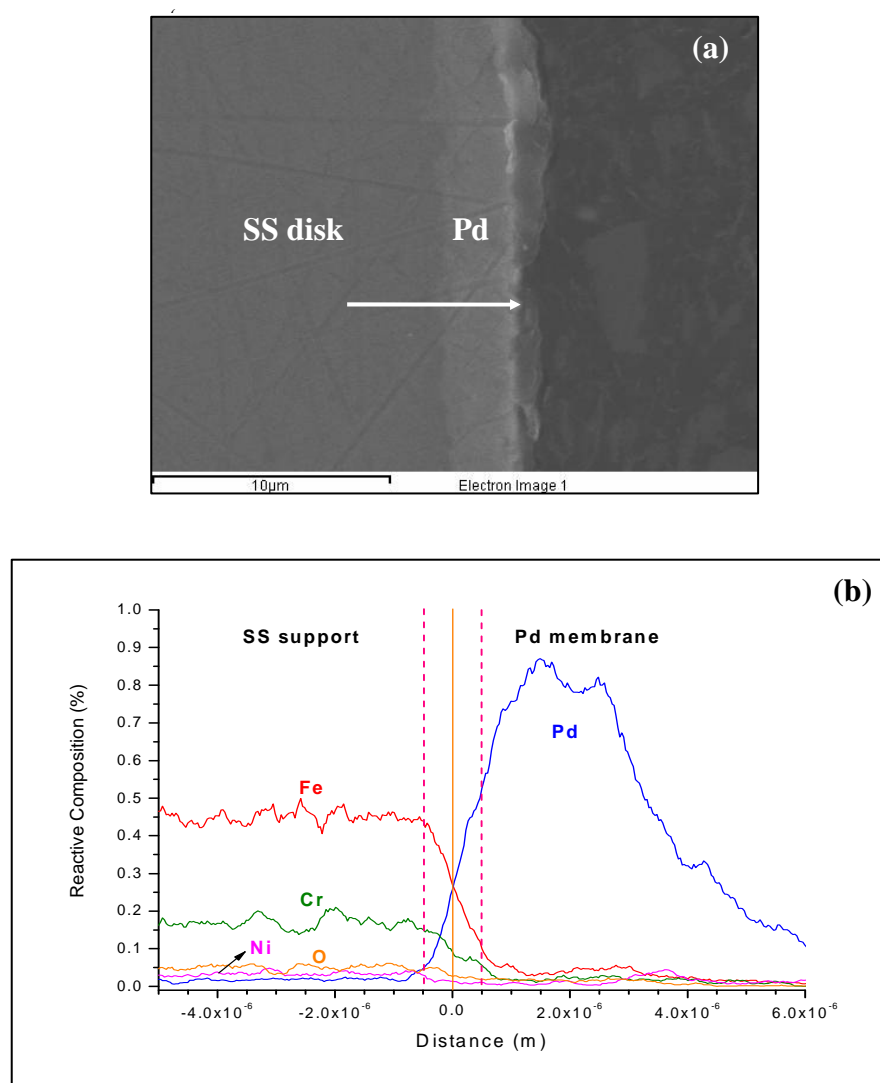


Figure 4.15 SEM micrograph (a) and EDS line scans (b) of Pd/TO-Cr₂O₃/SS (disk #06) after hydrogen exposure at 600°C for 24 hours

Figure 4.15 shows the EDS line scan of Pd/TO-Cr₂O₃/SS (disk #06) after hydrogen exposure at 600°C for 24 hours. It was found that not attributed of elemental in SS disk in Pd layer. Independent of the composition, the most important feature for oxide layer to be used as a barrier layer for Pd membrane is its stability under hydrogen atmosphere in long-term. The Cr₂O₃ has a high resistance to reduction under hydrogen atmosphere even at high temperature [37] but the Fe-rich top layer might get reduced in hydrogen atmosphere. In long-term stability, the inner oxide layer is a Fe-rich phase and reduction occurs, the effectiveness of the barrier layer not enough to prevent intermetallic diffusion completely.

Figures 4.16 - 4.17 shows the EDS line scan of Pd/EP-Cr₂O₃/SS (disks #12) and Pd/MS-Cr₂O₃/SS (disk #18) after hydrogen exposure at 600°C for 24 hours.

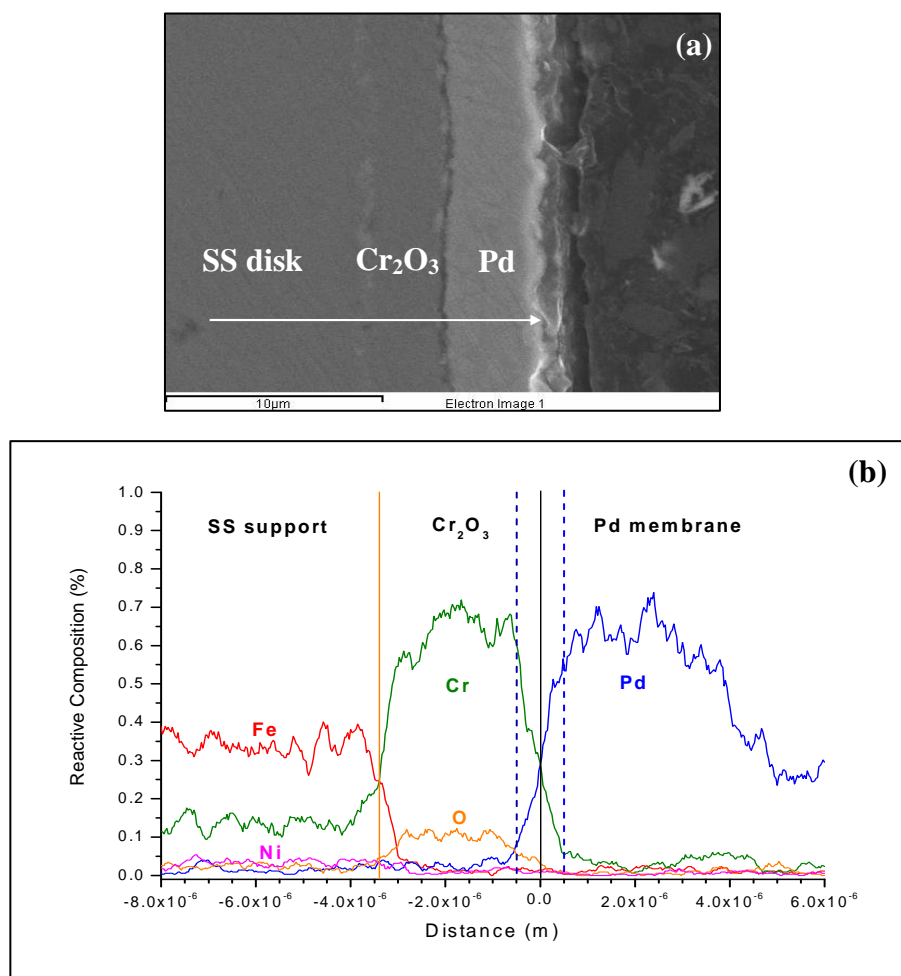


Figure 4.16 SEM micrograph (a) and EDS line scans (b) of Pd/EP-Cr₂O₃/SS (disk #12) after hydrogen exposure at 600°C for 24 hours

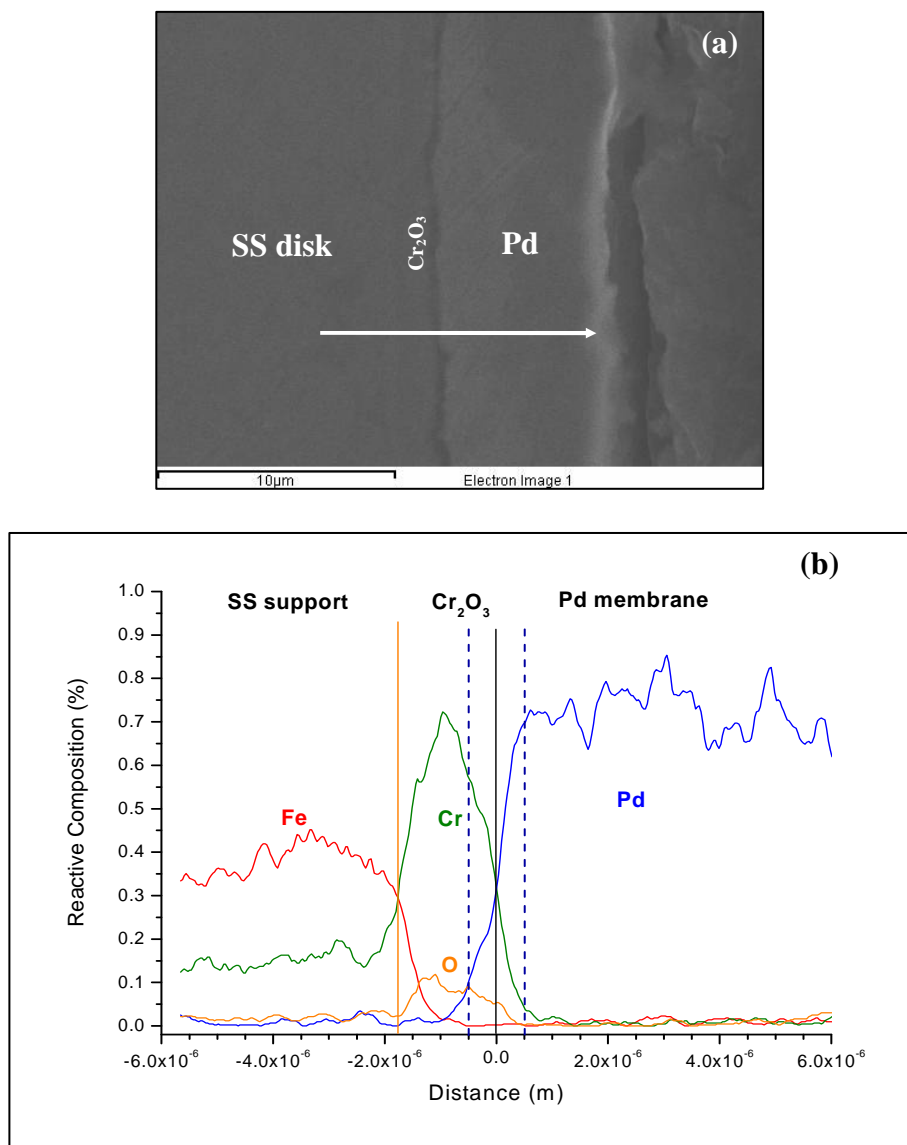


Figure 4.17 SEM micrograph (a) and EDS line scans (b) of Pd/MS-Cr₂O₃/SS (disk #15) after hydrogen exposure at 600°C for 24 hours

In Figures 4.16-4.17 shown the Cr₂O₃ thin films prepare by the EP and MS methods. The thickness of Cr₂O₃ barriers were approximate 2 μm. After hydrogen exposure at 600°C, It was found that not elemental of SS disks distribution in the Pd layers. When thickness of the barrier decrease, was approximate 1 μm, could be used to intermetallic diffusion barrier, show in Figure 4.18.

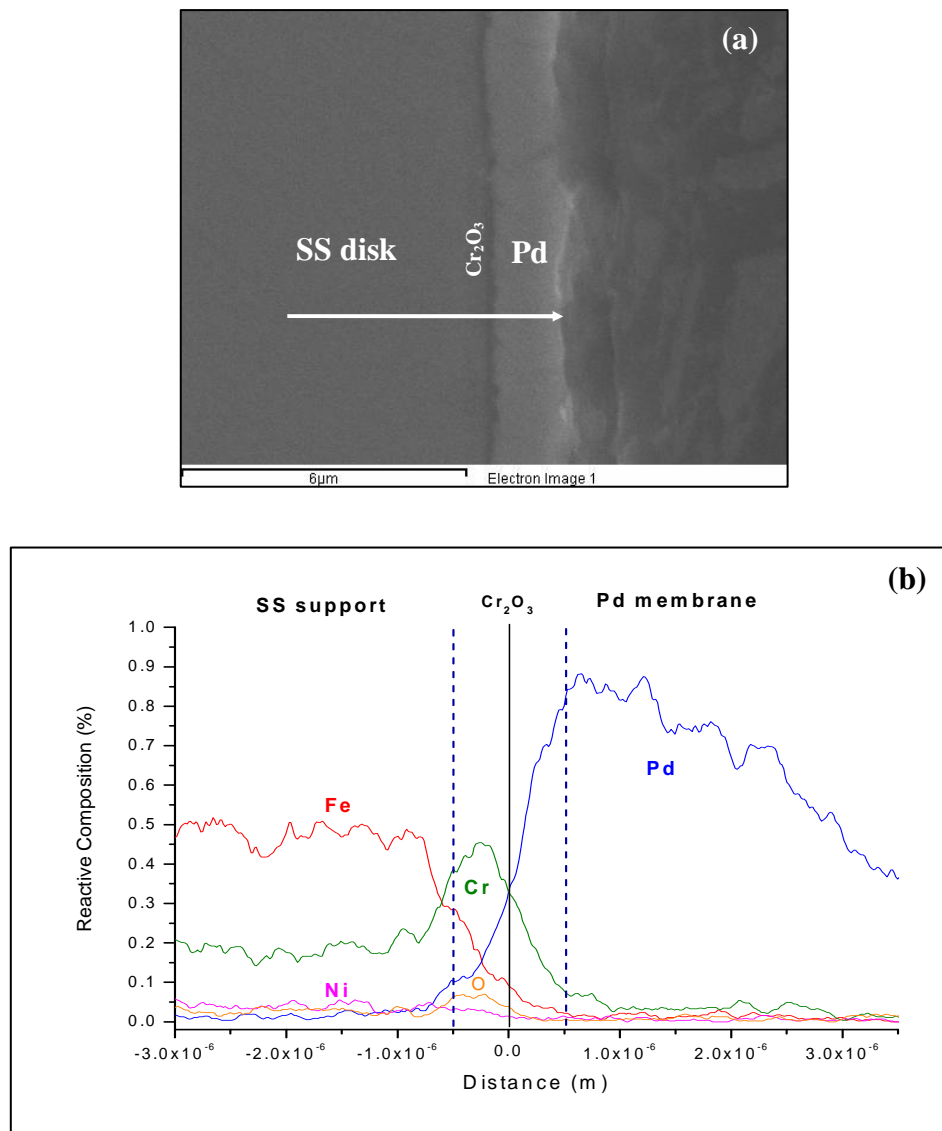


Figure 4.18 SEM micrograph (a) and EDS line scans (b) of Pd/Ms-Cr₂O₃/SS (disk #18) after hydrogen exposure at 600°C for 24 h

The results of all samples (disks #07 - #17) were not attributed of elemental in SS disk in Pd layer as same as the Pd/Ms-Cr₂O₃/SS (disk #18).

Figure 4.19 shows the SEM micrograph and EDS line scans of Pd/MS-CrN/SS (disk #24) after hydrogen exposure at 600°C for 24 hours. The thickness of CrN barriers were varies 3 μm (disks #19 - #21) to 2 μm (disks #22- #24). After hydrogen exposure at 600°C, It was found that not elemental of SS disks distribution in the Pd layers.

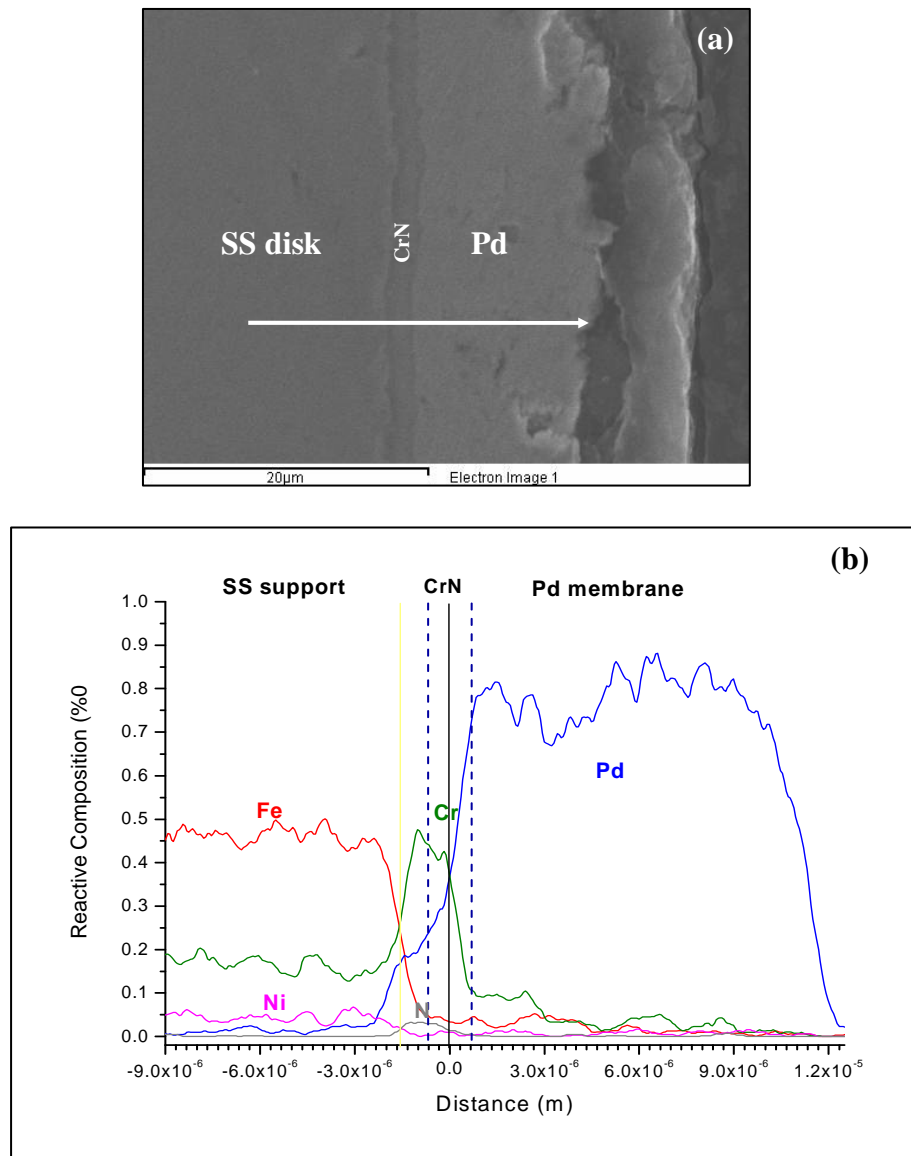


Figure 4.19 SEM micrograph (a) and EDS line scans (b) of Pd/MS-CrN/SS (disk #24) after hydrogen exposure at 600°C for 24 hours

The oxygen peak, nitrogen peak and high content of Cr in the interlayer for Figures 4.16- 4.19 to be confirm of the Cr_2O_3 and CrN thin flim formations.

From this study, it can be concluded that Cr_2O_3 and CrN layer with 1-1.5 μm thickness could suppress used as intermetallic barrier for metallic diffusion on palladium membrane at 400-600°C.

4.3 Hydrogen permeation flux testing

The permeation of hydrogen gas was measured at different temperature and pressures, carried out at 350, 400, 450 and 500°C for different pressures, respectively. The PSS disk was used as the support for hydrogen permeation flux test. The Pd membranes plated on the PSS disk as well as those on Cr₂O₃ and CrN thin films. Preliminary testing for dense Pd membranes was carried with helium gas at room temperature at pressures different up to 3 atm. If helium flux at the gas outlet could be detected, it meant that the not dense and had to plated again. The thickness of the palladium layer was calculated by the gravimetrically method and was assessed with their SEM micrographs.

The preparation conditions of the intermetallic diffusion barriers used in this study are summarized in Table 4.6.

Table 4.6 The preparation conditions of the intermetallic diffusion barriers

Disk no.	Synthesis type	Thickness of barrier (μm)	Thickness of Pd layer (μm)	
			gravimetric method	SEM
#25	-	-	31.32	31.0
#26	TO method of PSS disk	Too thin	47.26	42.67
#27	Cr ₂ O ₃ by EP method	2	36.21	34.88
#28	Cr ₂ O ₃ by MS method	2	31.53	29.23
#29	CrN by MS method	2	48.09	49.12

Prior to the hydrogen permeation tests, the Pd membrane was heat in helium at a rate of about 4°C/min. The hydrogen permeation flux and hydrogen permeance of dense Pd membranes were calculated according to the following equation:

$$\text{hydrogen permeation flux} \left(\frac{m^3}{m^2 h} \right) = \left(\frac{\text{flow rate of hydrogen gas} \left(\frac{ml}{min} \right)}{\text{active surface area} (cm^2)} \right) \times 0.6$$

$$\text{hydrogen permeance} \left(\frac{m^3}{m^2 h atm^{0.5}} \right) = \left(\frac{\text{hydrogen permeation flux} \left(\frac{m^3}{m^2 h} \right)}{P_{H_2 \text{ at shell side}}^{0.5} - P_{H_2 \text{ at tube side}}^{0.5} (atm^{0.5})} \right)$$

Figure 4.20 shows the surface micrographs of the Pd/PSS non barrier (disk #25) before and Pd/TO-Cr₂O₃/PSS (disk #26). It can be seen that the surface of disk #25 look smooth whereas the surface of disk #26 was much roughness. The surface of disks #25 - #26 as same as that the SS disk in 4.1.2.1.

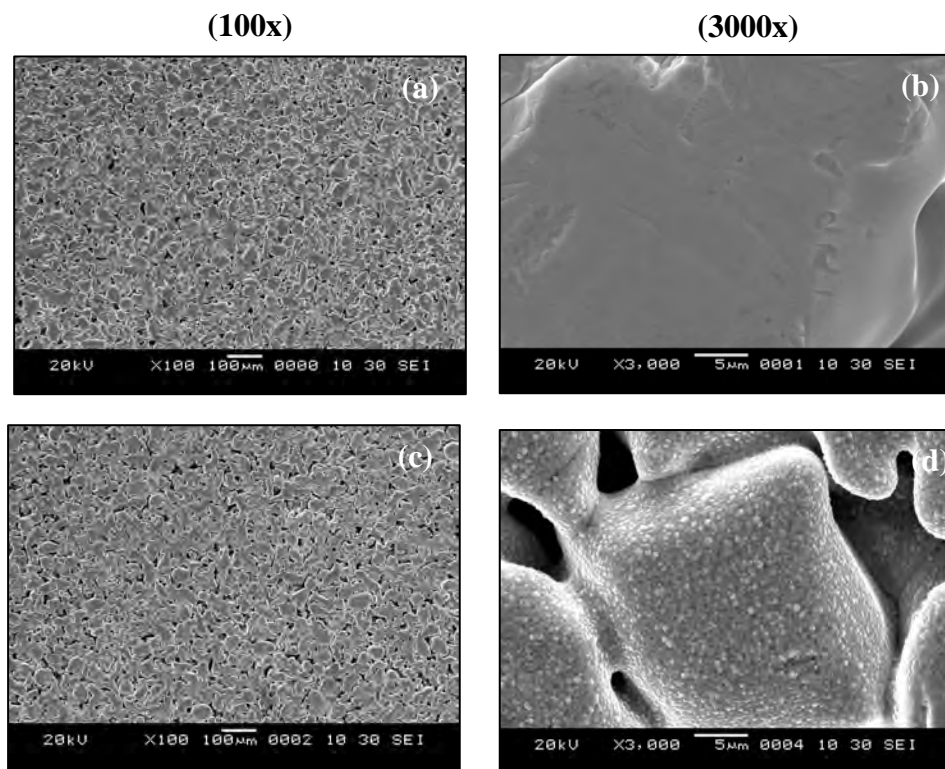


Figure 4.20 SEM micrograph of surface in the Pd/PSS non barrier (a, b) and Pd/TO-Cr₂O₃/PSS (c, d).

The surface micrographs of the different barriers obtained from the EP and MS methods on PSS disks are shown in Figure 4.21. The barrier is about 2 μm thick for all thin films. The surface of Cr₂O₃ thin film on the Pd/EP-Cr₂O₃/PSS (disk #27)

was round and rough. The other surface of Cr_2O_3 and CrN thin films by MS methods were appears continuous, smooth films and to bridge the pore openings in the PSS disks. In Figure 4.21, it was found that the Cr_2O_3 and CrN thin films were not decrease pinholes on PSS disks.

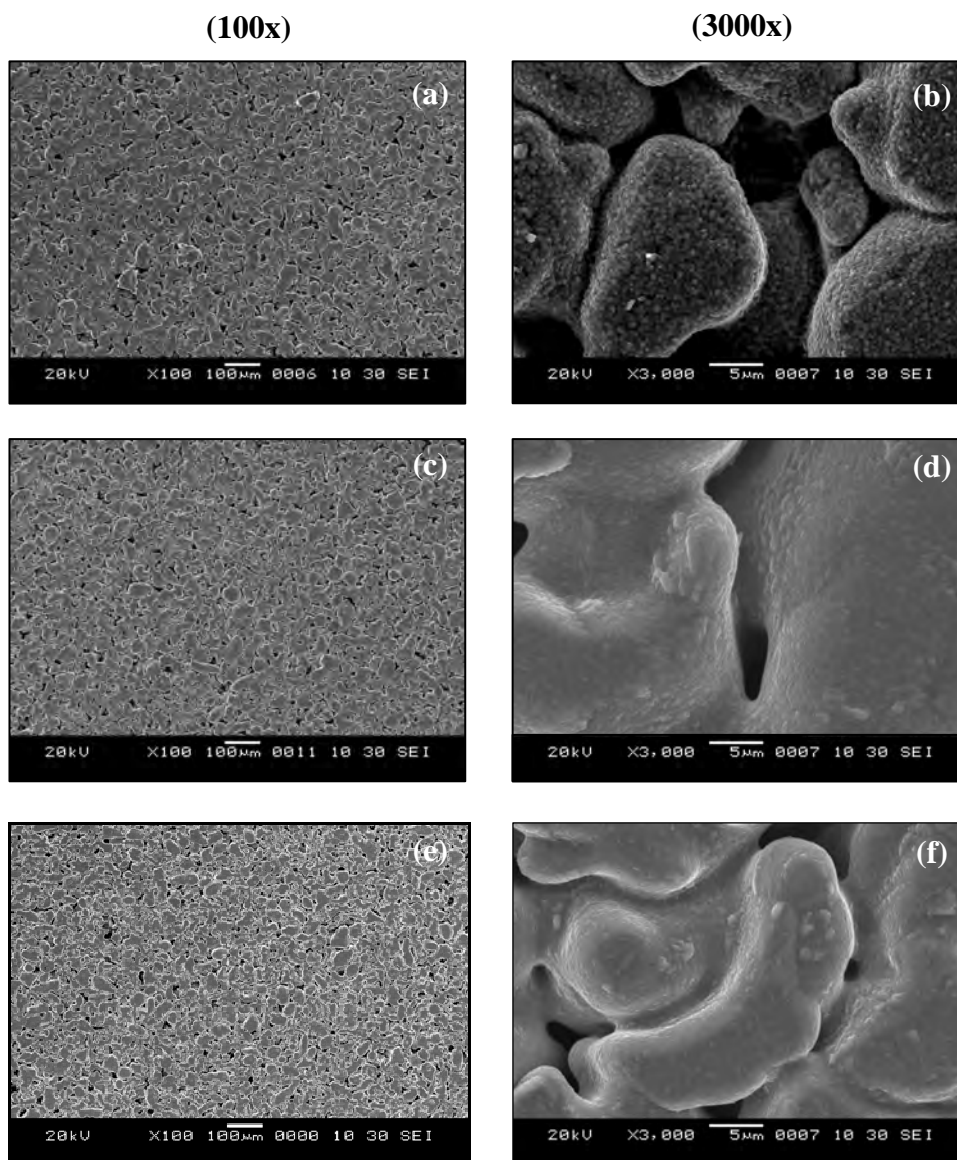


Figure 4.21 SEM micrograph of the Pd/TO-Cr₂O₃/PSS (a, b), Pd/EP-Cr₂O₃/PSS (c, d), and Pd/MS-Cr₂O₃/PSS (e, f).

Figure 4.22 (a) shows the dependence of the hydrogen flux with the transmembranes pressure differences at various temperatures for Pd/PSS non barrier (disk #25). The hydrogen flux increased with increasing temperature and differential pressure [16]. The same trend was observed for the Pd/TO-Cr₂O₃/PSS (disks #26) and Pd/EP-Cr₂O₃/PSS (disk #27) (Figure 2.4. b-e). This is consistent with the solution-diffusion mechanism of hydrogen through Pd membrane. Under this condition, the hydrogen flux should display a linear dependence on the difference of the square roots of inside and outside pressures. This is confirmed in Figure 4.23.

The hydrogen flux values obtained for Pd/PSS non barrier (disk #25) (Figure 4.22(a)) are lower than those disks. The lower hydrogen flux of disk #25 could be attributed to metallic interdiffusion between the Pd layer and PSS disk. In Figure 4.22 (e) shows that an increase of temperature steadily increases the permeance of Pd/MS-CrN/PSS (disk #29) until to 400°C where a further increase to 500°C does not substantially increase the hydrogen flux. The reason probably is the higher thickness of Pd membrane which leads to reduced permeance.

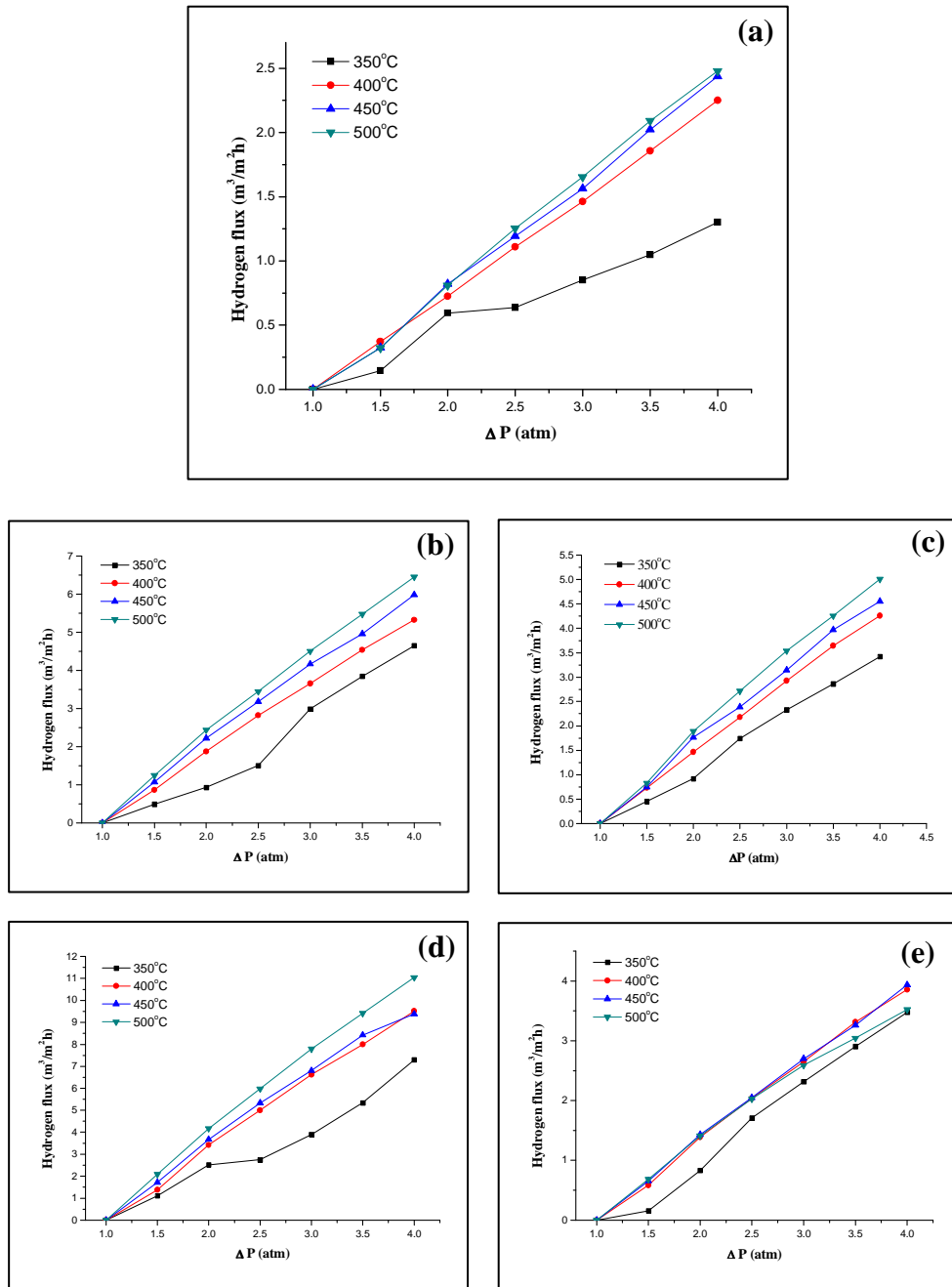


Figure 4.22 Permeation measurements at different temperature for disk #25 (a), disk #26(b), disk #27(c), disk #28 (d), and disk #29 (e)

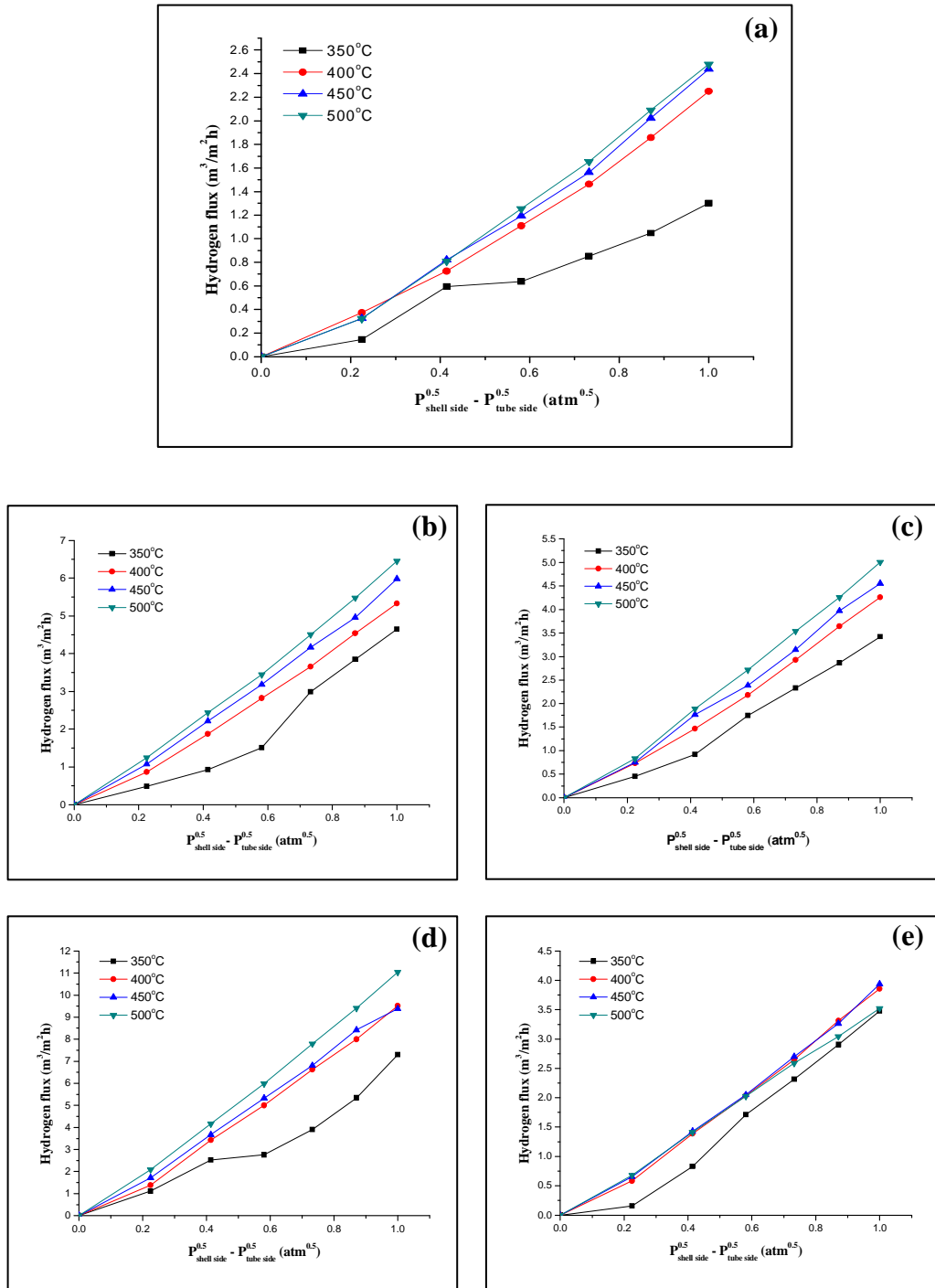


Figure 4.23 Permeation measurements to the hydrogen pressures for Pd/PSS (a), Pd/TO-Cr₂O₃/PSS (b), Pd/EP-Cr₂O₃/PSS (c), Pd/MS-Cr₂O₃/PSS (d), and Pd/Ms-Cr₂O₃/PSS (e)

The hydrogen flux and hydrogen permeance results for the prepared membranes at the different temperatures are summarized in Table 4.6. The hydrogen flux and hydrogen permeance of the Pd/MS-Cr₂O₃/PSS (disk #28) was the higher than those disks

Table 4.6 The hydrogen flux and hydrogen permeance of the composite membranes

Disk no.		Temperature (°C)			
		350	400	450	500
#25	H ₂ flux	1.30	2.25	2.44	2.48
	H ₂ permeance	1.36	2.42	2.68	2.78
#26	H ₂ flux	4.65	5.33	5.98	6.45
	H ₂ permeance	5.68	5.76	6.24	6.70
#27	H ₂ flux	3.42	4.26	4.55	5.07
	H ₂ permeance	3.92	4.60	4.88	5.33
#28	H ₂ flux	7.29	9.51	9.38	11.04
	H ₂ permeance	7.39	10.36	10.02	11.52
#29	H ₂ flux	3.47	3.85	3.94	3.52
	H ₂ permeance	4.34	4.21	4.17	3.65

A comparison of the hydrogen fluxes at 500°C as a function of the hydrogen pressure for all samples were give in Figure 4.24. Figure 4.24 (a) shows the linear relationship between the hydrogen pressure difference and the flux is assumed and Figure 4.24 (b) shows the hydrogen flux is expected to be proportional to the difference of the square root of the hydrogen pressure. Pd/MS-Cr₂O₃/PSS (Disk #28) is the only one for which the data suggest a linear relationship between the flux and pressure difference.

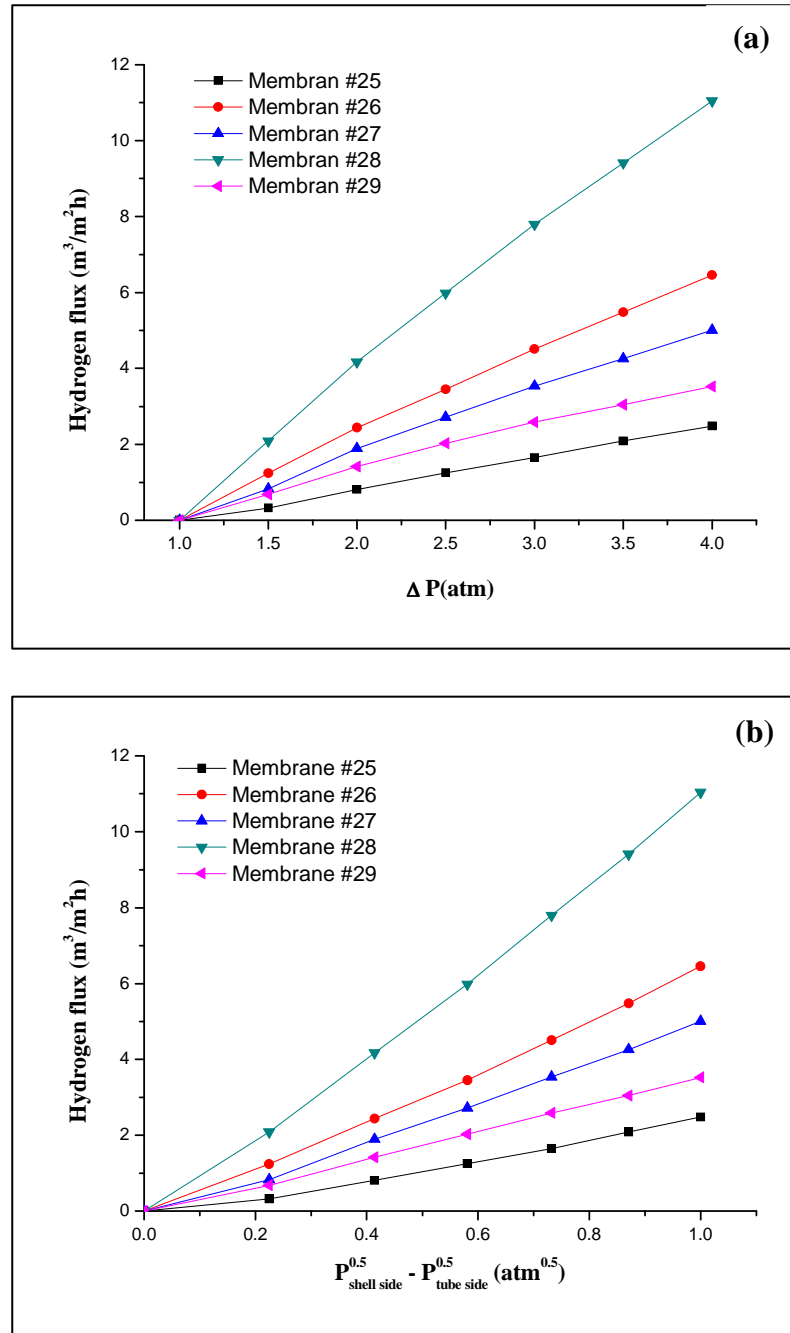


Figure 4.24 the linear relationship between the hydrogen pressure difference and the flux (a) and the hydrogen flux of the square root of the hydrogen pressure (b) for all samples.

CHAPTER V

SUMMARY AND CONCLUSIONS

The purpose of this study is to prepare chromium oxide (Cr_2O_3) and chromium nitride (CrN) diffusion barriers for stainless steel (SS) supported palladium (Pd) membrane. The thickness of thin films by electroplating and sputtering methods depended on the Cr deposition time. It was found that the mixed oxide layer consisted of Cr_2O_3 layer and Fe_2O_3 layer on top. The mixed oxide was increased with higher oxidation temperatures. The suitable oxidation temperature was therefore considered to be at 600°C for 6 hours. Sputtering produced films with finer grain and was better at least in term of precision of resulting layer thickness. However, it requires expensive equipment as opposed to the general equipment setting of electroplating. CrN thin films were produced from a pure chromium target in a mixing of argon and nitrogen pressure. The sputtering rate for the CrN thin film less than the rate for Cr thin film.

The Pd membranes were deposited on top of each thin film on SS disk by electroless plating. The thickness of Pd membrane depended on the plating time required until dense Pd membrane was obtained which was evaluated by helium flux measurement. Dense Pd membranes have the thickness $\sim 30\text{-}50\ \mu\text{m}$.

All Cr_2O_3 and CrN thin films acted as the good intermetallic diffusion barriers due to their performance on the protection palladium layer from intermetallic diffusion. In long-term stability, the Cr_2O_3 by thermal oxidation method might not be enough to inhibit intermetallic diffusion completely because of the iron oxide rich top layer might get reduced in hydrogen atmosphere. Moreover, the thickness of Cr_2O_3 and CrN thin films as low as $1\ \mu\text{m}$ showed as the effective intermetallic diffusion barriers. In addition, Cr_2O_3 prepared by sputtering exhibited the highest hydrogen permeance.

5.1 Further Works

- 5.1.1 Prepare Cr_2O_3 layer by Cr-reactive sputtering in oxygen atmosphere and determine its performance on intermetallic diffusion inhibition comparing with other methods of preparation.
- 5.1.2 Test long-term stability of hydrogen permeation flux of the palladium membrane containing each type of intermetallic diffusion barriers.

REFERENCES

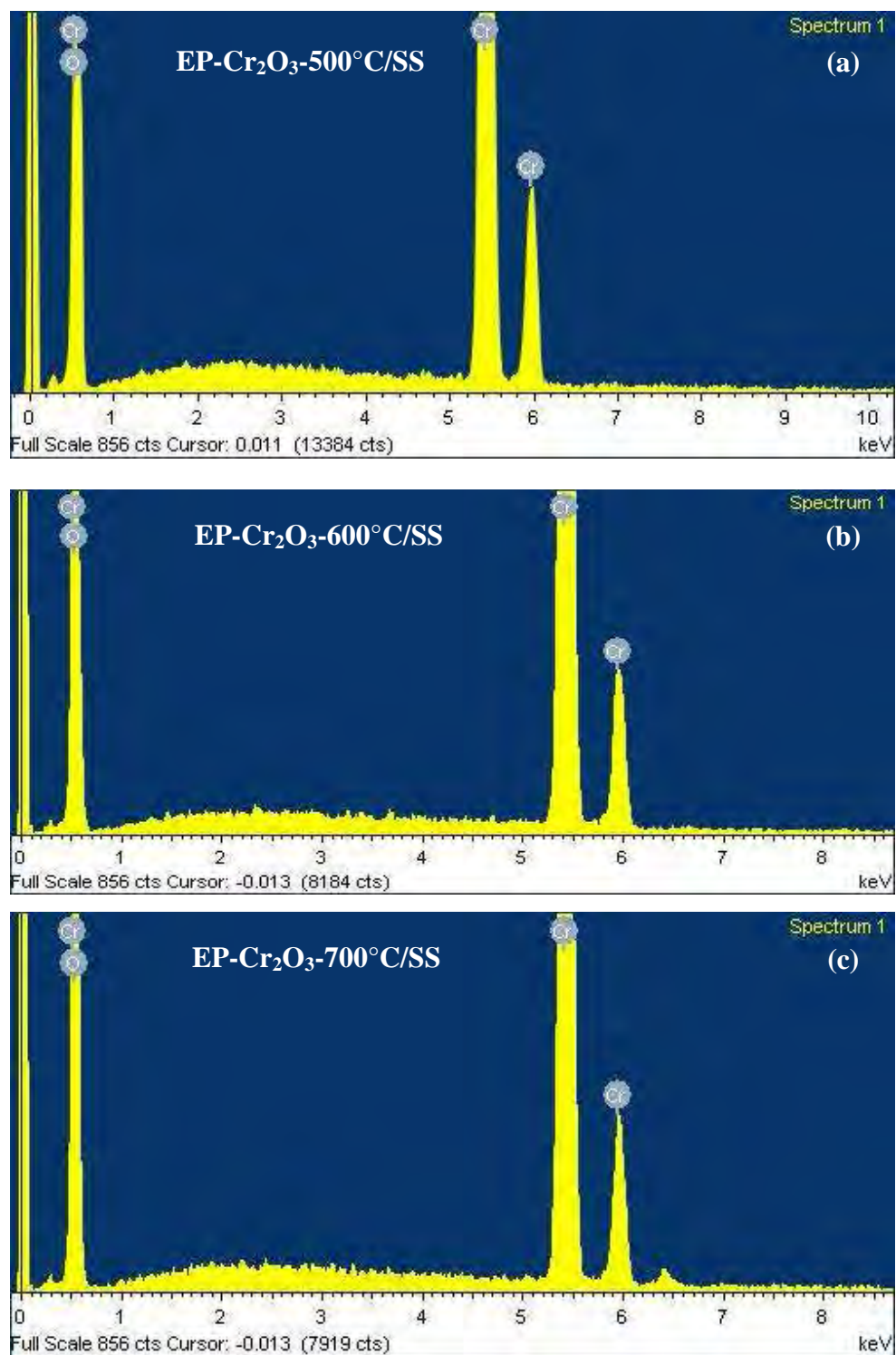
- [1] Uemiya, S. State-of-the-art of supported metal membranes for gas separation. Separation and Purification Methods 28 (1999): 51-85.
- [2] Paglieri, S. N. and Way, J. D. Innovations in palladium membrane research. Separation and Purification Methods 31 (2002): 1-169.
- [3] Bryden, K. J. and Ying, J. Y. Nanostructured palladium-iron membranes for hydrogen separation and membrane hydrogenation reactions. Journal of membrane Science 203 (2002): 29-42.
- [4] Cheng, Y.S. and Yeung, K. L. Palladium-silver composite membranes by electroless plating technique. Journal of membrane Science 158 (1999): 127-141.
- [5] Jun, C. S. and Lee, K. H. Palladium and Palladium alloy composite membranes prepared by metal-organic vapor deposition method (cold-wall). Journal of membrane Science 176 (2000): 121-130.
- [6] Mardilovich, P. P., She, Y. H., Ma, Y. H. and Rei, M.H. Defect free palladium membrane on porous stainless steel support. AIChE Journal 44 (1998): 310-322
- [7] O'Brien, J., Hughes, R. and Hisek, J. Pd/Ag membranes on porous alumina substrates by unbalanced magnetron sputtering. Surface and Coatings Technology 142-144 (2001): 253-259.
- [8] Tosti, S., Bettinali, L., Castelli, S., Sarto, F., Scaglione, S. and Violante, V. Sputtered electroless, and rolled palladium-ceramic membranes. Journal of membrane Science 196 (2002): 241-249.
- [9] Li, A., Grace, J. R., Lim, C. J. Preparation of thin Pd-based composite membrane on planar metallic substrate. Part I. The pre-treatment of the porous stainless steel substrate. Journal of membrane Science 192 (2007): 175-181.

- [10] Wang, D., Tong, H. H., Xu, H. Y., Matsumura, Y. Preparation of palladium membrane over porous stainless steel tube modified with zirconium oxide. Catalysis Today 93-95 (2004): 689-693.
- [11] Zhang, K., Gao, H., Rui, Z., Liu, P., Li, Y. and Lin, Y. S. High-temperature stability of palladium membranes on porous metal supports with different intermediate layers. Industrial & Engineering Chemistry Research 48 (2009): 1880-1886.
- [12] Ma, H.Y., and others. Characterization of Intermetallic Diffusion Barrier and Alloy Formation for Pd/Cu and Pd/Ag Porous Stainless Steel Composite Membranes. Industrial & Engineering Chemistry Research 43 (2004): 2936-2945.
- [13] Huang, H. and Dittmeyer, R. Preparation and characterization of composite palladium membranes on sinter-metal supports with a ceramic barrier against intermetallic diffusion. Journal of membrane Science 282 (2006): 296-310.
- [14] Ayturk, M. E., Mardilovich, I. P., Engwall, E. E. and Ma, Y. H. Synthesis of composite Pd-porous stainless steel (PSS) membranes with a Pd/Ag intermetallic diffusion barrier. Journal of membrane Science 285(2006): 385-394.
- [15] Greeff, A. P., Louw, C. W. and Swart, H. C. The oxidation of industrial FeCrMo steel. Corrosion Science 42(2000):1725-1740.
- [16] SaTo, I., and others. Oxidation behavior of modified SUS316 (PNC316) stainless steel under low oxygen partial pressure. Journal of Nuclear Materials 304 (2002): 21-28.
- [17] Lacoste, A., Bechu, S., Arnal, Y., Pelletier, J. and Gouttebaron, R. Plasma-based ion implantation of oxygen in stainless steel: influence of ion energy and dose. Surface and Coatings Technology 156 (2002): 225-228.
- [18] Sabioni, A. C. S., Huntz, A. M., Silva, F. and Jomard, F. Diffusion of iron in Cr₂O₃: polycrystals and thin films. Materials Science and Engineering:A 392 (2005): 254-261.

- [19] Huntz, A. M., and others. Oxidation of AISI 304 and AISI 439 stainless steel. Materials Science and Engineering:A 447 (2007): 266-276.
- [20] Wang, P. W., Jin-Cherng, H. and Luu-Gen, H. Metallic phase formation in oxide films. Journal of Non-crystalline Solids 354 (2008): 1256-1262.
- [21] Eun-Suok Oh, O. Kinetic and kinematic for the metal oxidation on a sphere geometry. Chemical Engineering Journal 135 (2008): 157-167
- [22] Stefanov, P., Stoychev, D., Stoycheva, M. and Marinova, Ts. XPS and SEM studies of chromium oxide films chemically formed on stainless steel 316L. Materials Chemistry and Physics 65 (2000): 212-215.
- [23] Longhai, S., Xu, S., Sun, N. and Taimin, C. Synthesis of nanocrystalline CrN by arc discharge. Materials Letters 62 (2008): 1469-1471.
- [24] Shu, J., Adnot, A., Grandjean, B.P.A. and Kaliaguine, S. Structurally stable composite Pd-Ag alloy membranes: Introduction of a diffusion barrier. Thin Solid films 289 (1996): 72-79.
- [25] Yepes, D., Cornaglia, L.M., Irusta, S. and Lombardo, E.A. Different oxides used as diffusion barrier in composite hydrogen permeable membranes. Journal of membrane Science 274(2006): 92-101.
- [26] Suthewawat, S., Supawan, T. and Ma, Y.H. Chromium oxide intermetallic diffusion barrier for palladium membrane supported on porous stainless steel. Journal of membrane Science 347(2010): 8-16.
- [27] Zhang, Z. G., and others. Control of microstructures and properties of dc magnetron sputtering deposited chromium nitride films. Vacuum 82 (2008): 501-509.
- [28] De Souza, S. D., Olzon-Dionysio, M., Miola, E. J. and Paiva-Santo, C. O. Plasma nitriding of sintered AISI 316L at several temperatures. Surface and Coatings Technology 184 (2004): 176-181.
- [29] Xu.Nanping, L., Xue, F., Yiqua, J., Wanqin, H. and Yan, S. Effect of EDTA on preparation of Pd membranes by photocatalytic deposition. Desalination 192 (2006): 177-124.

- [30] Mardilovich, I. P., Engwall, E. and Ma, Y.H. Dependence of hydrogen flux on the pore size and plating surface topology of asymmetric Pd-porous stainless steel membranes, Desalination 144 (2002): 85-89.
- [31] Su, C., Jin, T., Kuraoka, K., Matsumura, Y. and Yazawa, T. Thin palladium film supported on SiO₂-modified porous stainless steel for a high-hydrogen-flux membrane, Industrial & Engineering Chemistry Research 44 (2005): 3053-3058.
- [32] Rothenberger, K. S., and others. High pressure hydrogen permeance of porous stainless steel coated with a thin palladium film via electroless plating. Journal of Membrane Science 344 (2004): 55-59.
- [33] Guazzone, F., Ayturk, M. E. and Ma, Y. H. Effect of intermetallic diffusion barrier on the stability of composite Pd/PSS membrane at high temperature. 21st Annual International Pittsburgh Coal Conference—Coal, Energy and the Environment. Osaka, Japan. 2004, pp.9-11.
- [34] Navinsek, B., Panjan, P. and Cvelbar, A. Characterization of low temperature CrN and TiN (PVD) hard coating. Surface and Coatings Technology 74-75 (1995): 155-161.
- [35] Shibagaki, S., Koga, A., Shirakawa, Y., Onishi, H., Yokokawa, H. and Tanaka, J. Chemical reaction path for thin film oxidation of stainless steel. Thin Solid Films 303 (1997): 101-106.
- [36] Sivaraman, G., Raj, B., Jayakumar, T. Oxidation behavior of type 316 stainless steel in the temperature range 873-1073K. Transactions of the Indian Institute of Metals 37(1984): 356-365.
- [37] Samsanov, G. V. The Oxide Handbook. IFI/Plenum. New York. Washington. DC. London. 1973.

APPENDICX

Intermetallic diffusion barrier test

FigureA1. EDS spectrum for EP-Cr₂O₃-500°C/SS (a), EP-Cr₂O₃-600°C/SS (b) and EP-Cr₂O₃-700°C/SS (c)

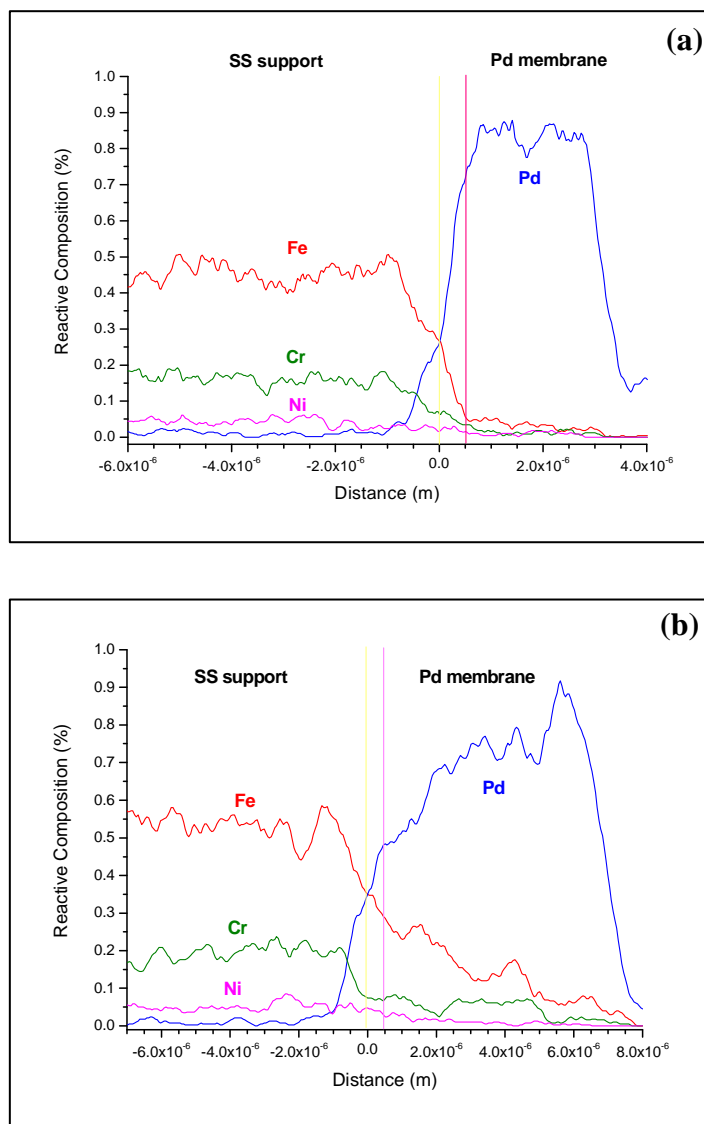


Figure A2. The EDS line scans of Pd membrane samples in fresh state (a) and after treatment at 400° (b), 500° (c), and 600°C (d) after 24 hours.

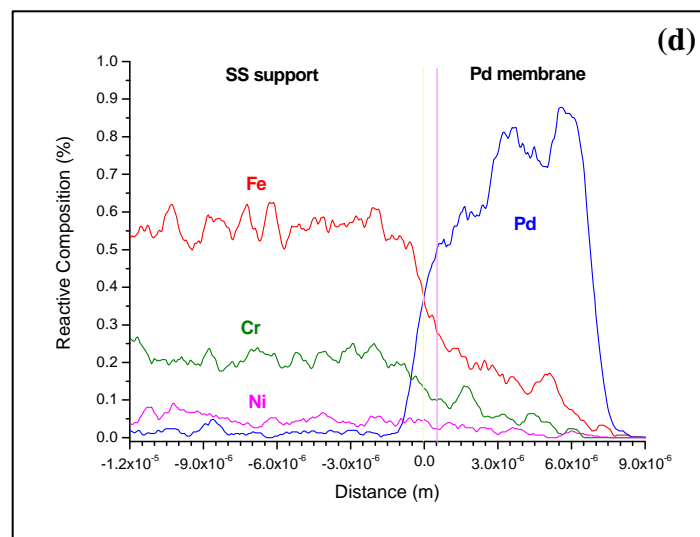
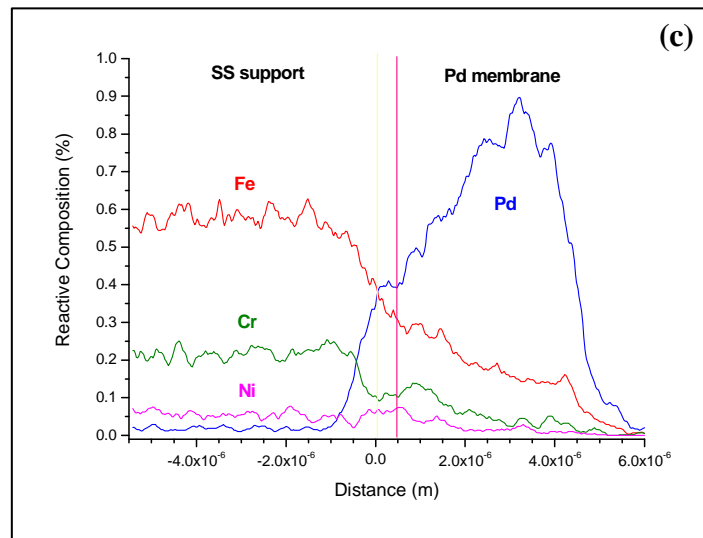


Figure A2. (Continued)

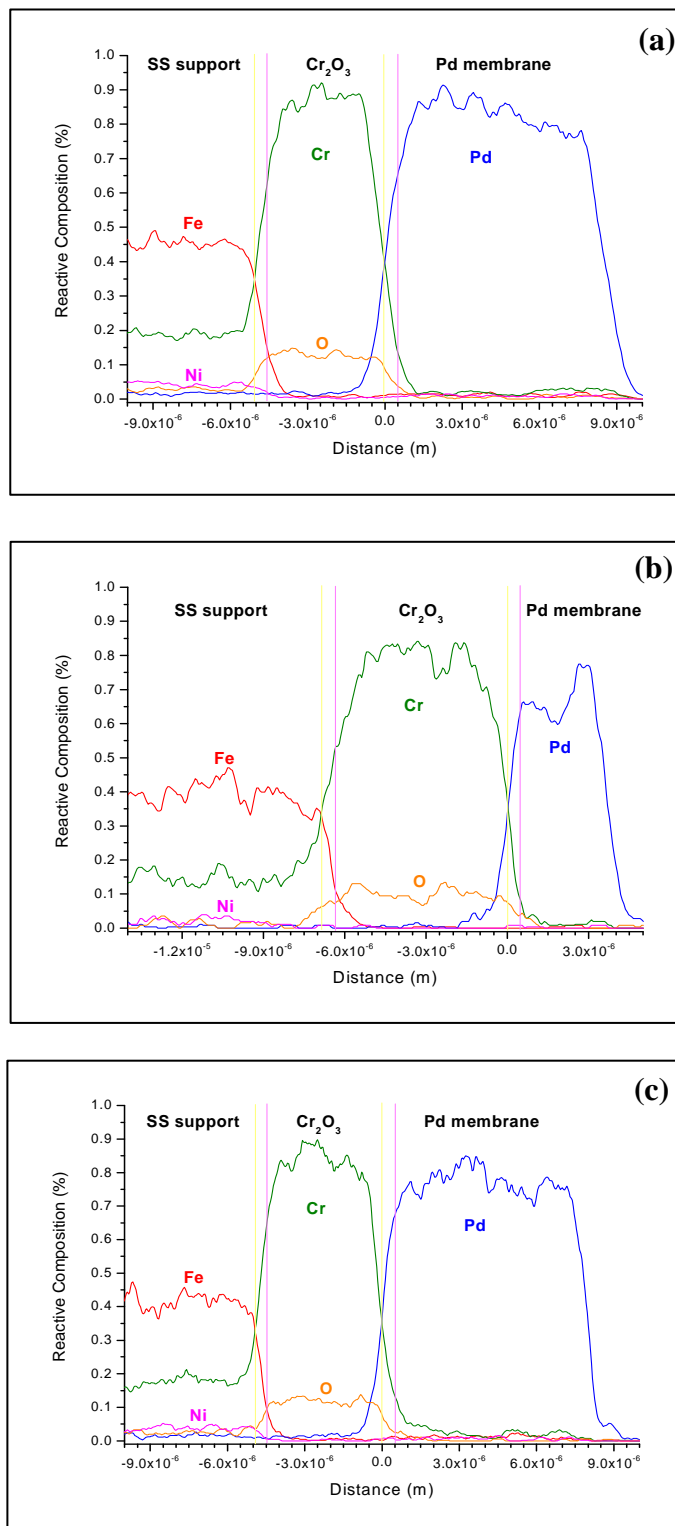


Figure A3. The EDS line scans of Pd/EP-Cr₂O₃-1.0 min-600°C/SS membrane samples after 24 h hydrogen exposure at 400° (a), 500° (b), and 600°C (c)

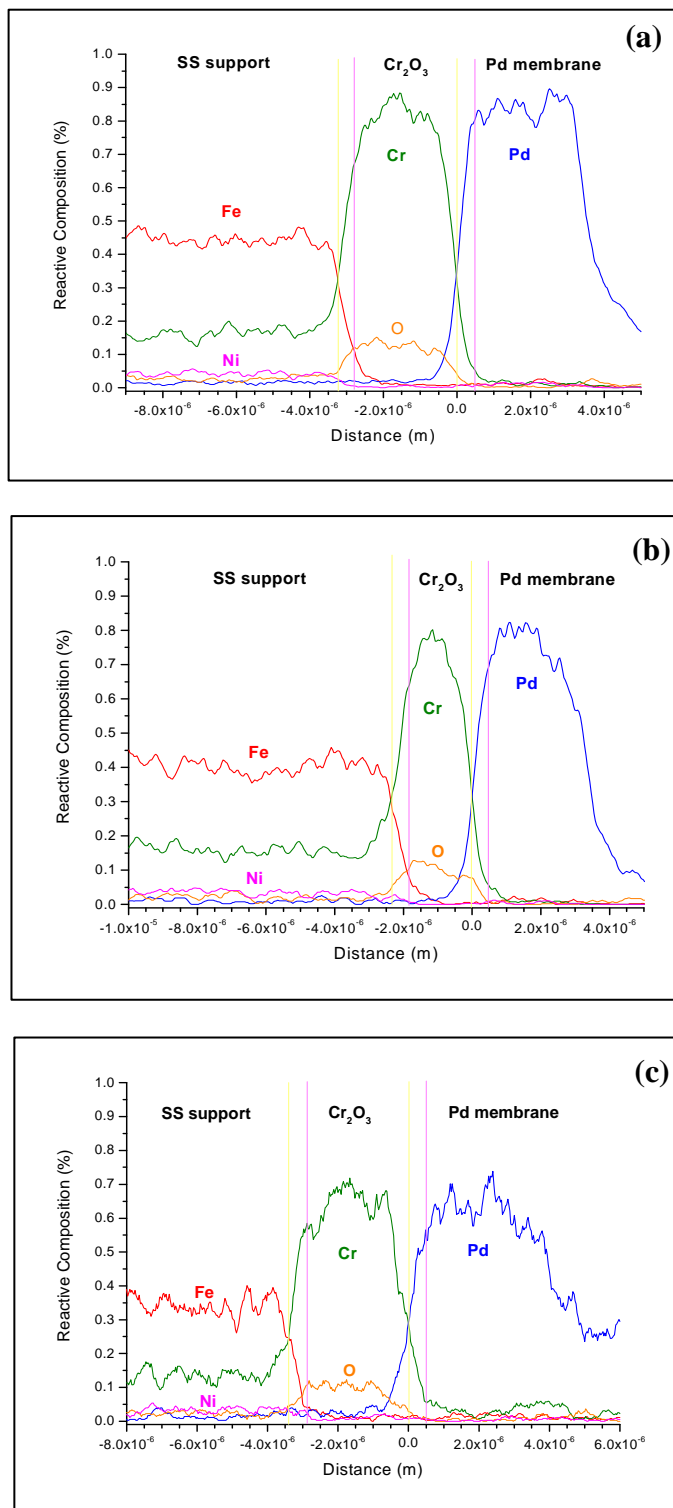


Figure A4. The EDS line scans of Pd/EP- Cr_2O_3 -0.5 min-600°C/SS membrane samples after 24 h hydrogen exposure at 400° (a), 500° (b), and 600°C (c)

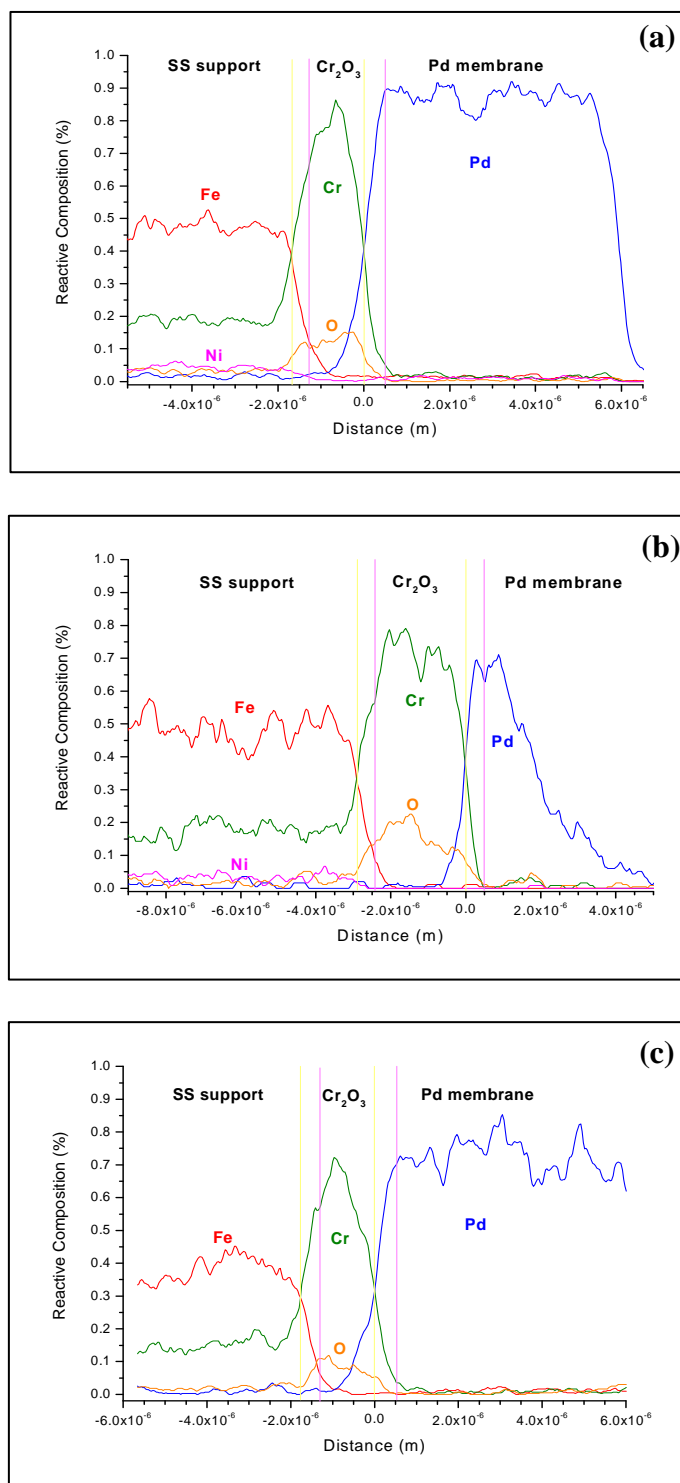


Figure A5. The EDS line scans of Pd/MS- Cr_2O_3 -45 min-600°C/SS membrane samples after 24 h hydrogen exposure at 400° (a), 500° (b), and 600°C (c)

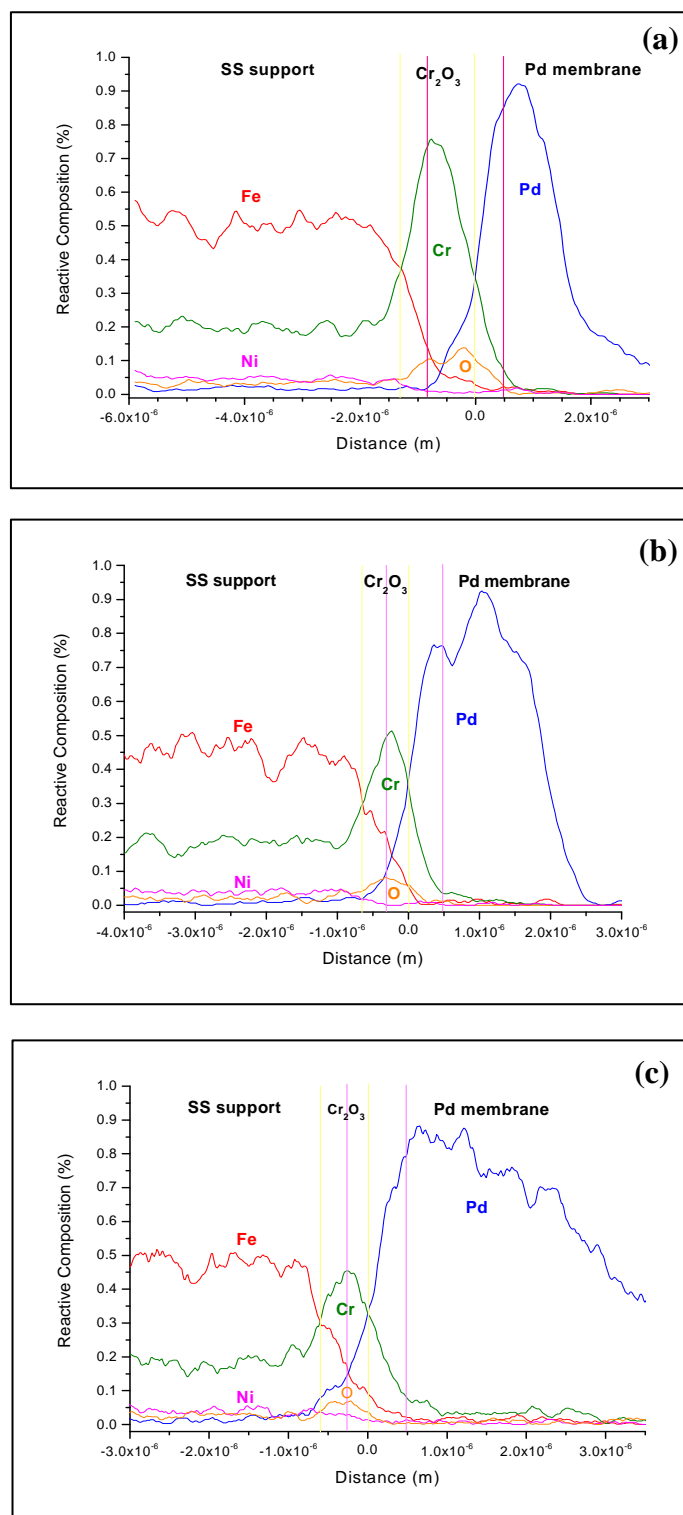
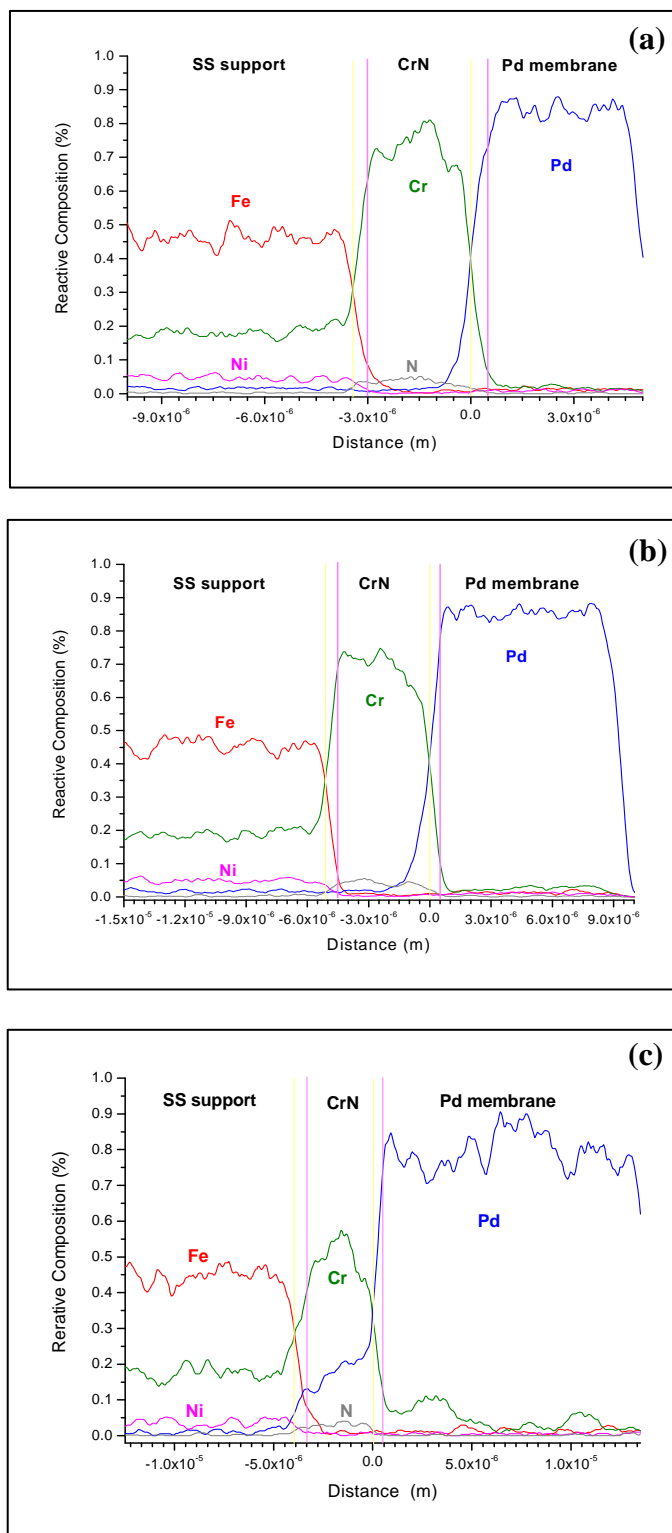


Figure.A6 The EDS line scans of Pd/MS-Cr₂O₃-15 min-600°C/SS membrane samples after 24 h hydrogen exposure at 400° (a), 500° (b), and 600°C (c)



FigureA7. The EDS line scans of Pd/MS-CrN-60 min/SS membrane samples after 24 h hydrogen exposure at 400° (a), 500° (b), and 600°C (c)

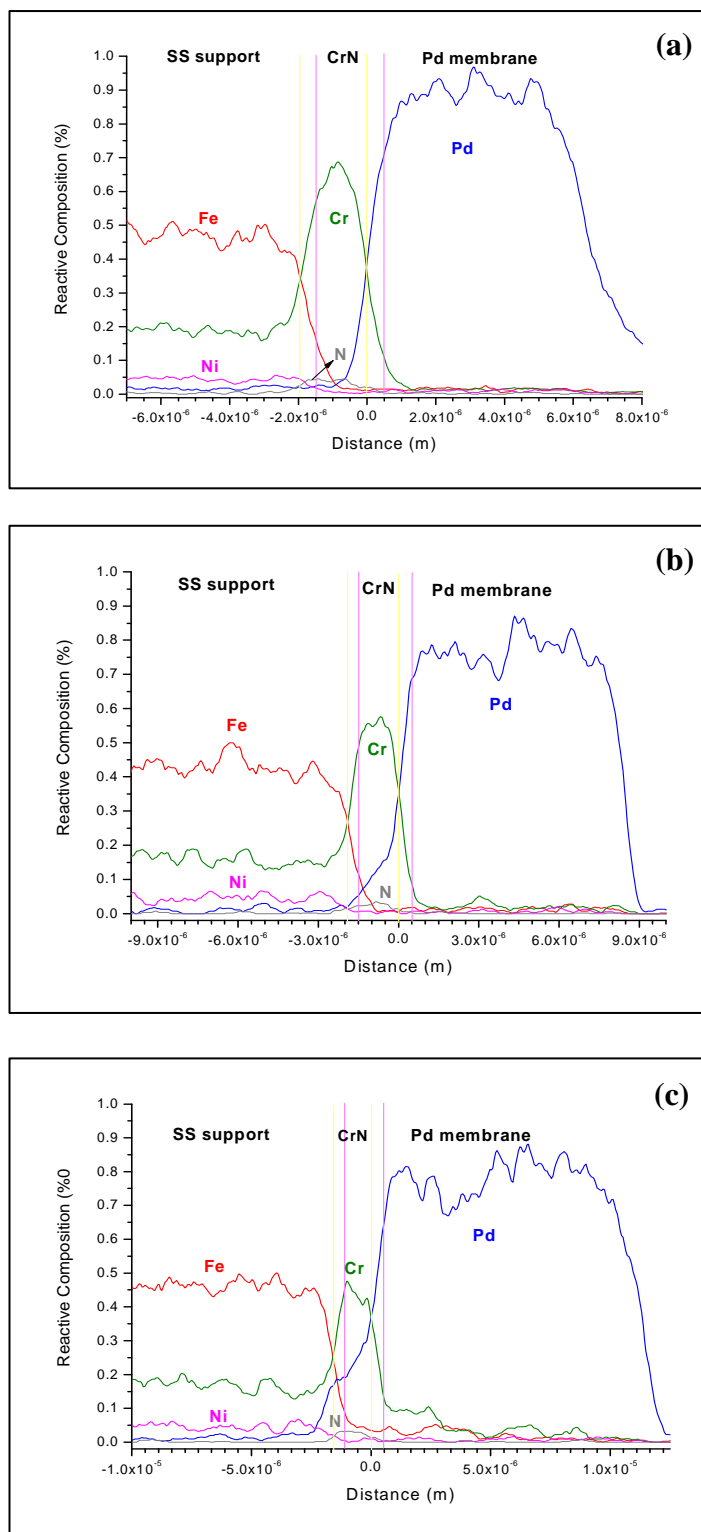


Figure A8. The EDS line scans of Pd/MS-CrN-30 min/SS membrane samples after 24 h hydrogen exposure at 400° (a), 500° (b), and 600°C (c)

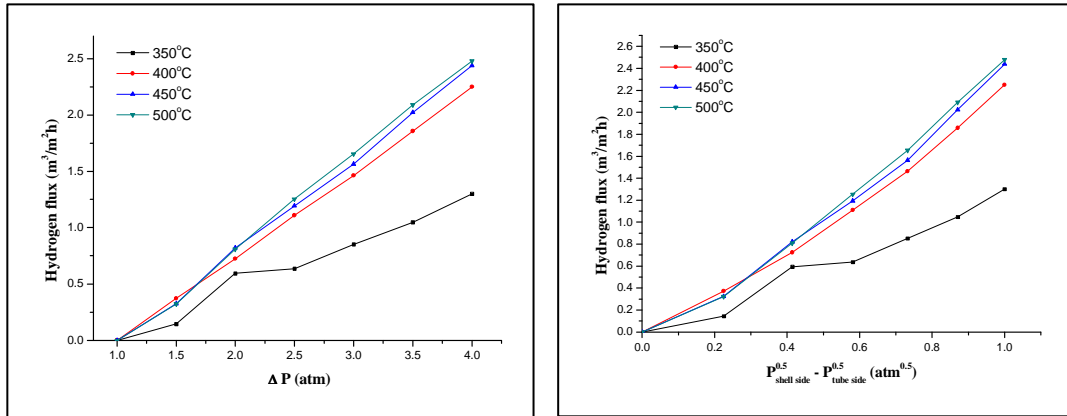


Figure A9. The linear relationship between the hydrogen pressure difference and the flux (a) and the hydrogen flux of the square root of the hydrogen pressure (b) for disk #25

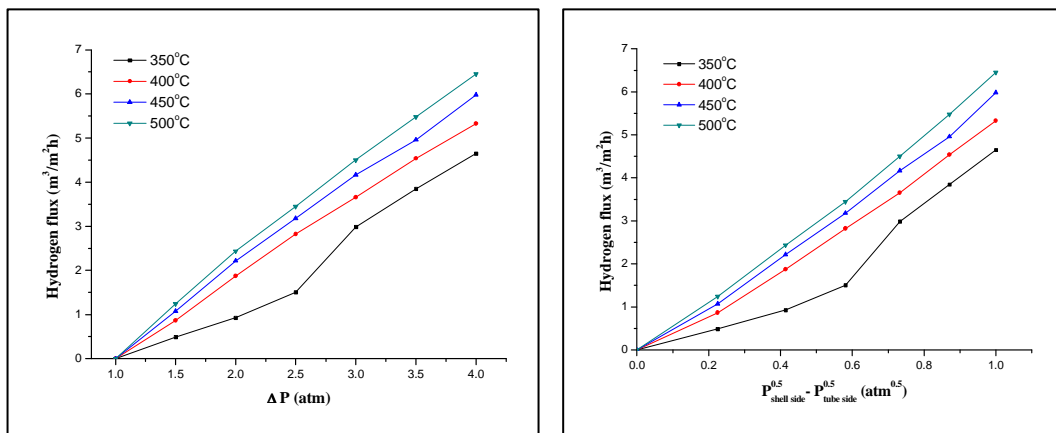


Figure A10. The linear relationship between the hydrogen pressure difference and the flux (a) and the hydrogen flux of the square root of the hydrogen pressure (b) for disk #26

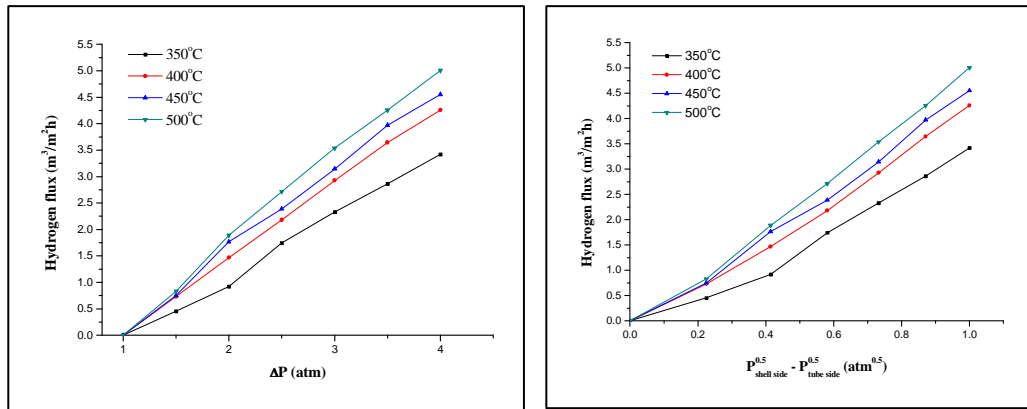


Figure A11. The linear relationship between the hydrogen pressure difference and the flux (a) and the hydrogen flux of the square root of the hydrogen pressure (b) for disk #27

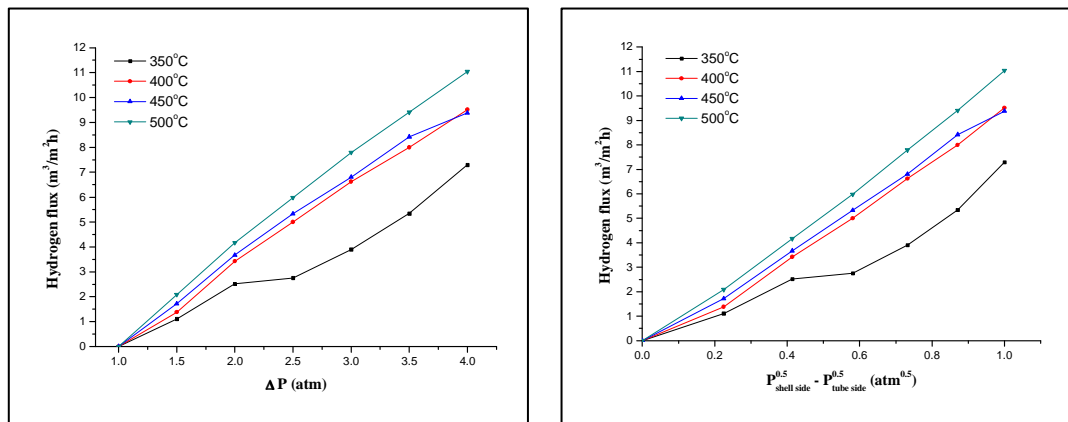


Figure A12. The linear relationship between the hydrogen pressure difference and the flux (a) and the hydrogen flux of the square root of the hydrogen pressure (b) for disk #28

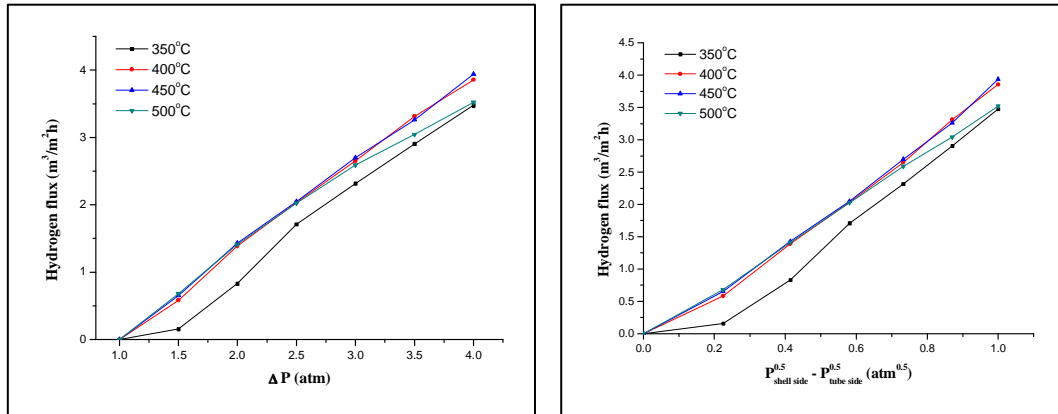


Figure A13. The linear relationship between the hydrogen pressure difference and the flux (a) and the hydrogen flux of the square root of the hydrogen pressure (b) for disk #29

VITAE

- Name:** Miss Saranya Ploypardup
- Date of Birth:** June 13, 1985
- Residence:** 100/3 Moo 8, Tambon Mathong, A.Phrompiram, Phitsanulok
65180
- Education:**
In 2006 Bachelor of Science (Chemistry), Naresuan University,
Phitsanulok, Thailand.
- Presentation**
In 2009 Saranya Ploypardup, Supawan Tantayanon and Sukkaneste
Tunkasamitra, "Preparation of CrN diffusion barrier for
stainless steel supported palladium membrane, The 35rd
Congress on Science and Technology of Thailand, Faculty of
Science , Burapha University ,Thailand.